RECOVERY OF HYDROGEN AND HELIUM FROM THEIR MIXTURES USING METAL HYDRIDES

by

MUZAFFER TONGUC OZTEK

B.S. Middle East Technical University, 1999

A thesis submitted in partial fulfillment of the requirements
for the degree of Master of Science
in the Department of Chemistry
in the College of Arts and Sciences
at the University of Central Florida
Orlando, Florida

Summer Term
2005

ABSTRACT

Waste streams of hydrogen and helium mixtures are produced at the Kennedy Space Center during purging of the hydrogen systems and supply lines. This process is done prior to and after hydrogen servicing. The purged waste gases are lost to the atmosphere, resulting in an annual loss of 2 million and 0.1 million standard cubic meters of helium and hydrogen, respectively. Recovery of these gases will have an economic benefit. Metals, alloys, and intermetallics are known to react with hydrogen in favorable conditions; therefore, they have the possibility of serving as separating and recovery agents.

In this study, Mg_2Ni, VTiNi and $LaNi_5$ were studied for the separation of H_2 from He, using differential scanning calorimetry and thermal volumetric analysis. The ability of $LaNi_5$ to react with hydrogen reversibly at room temperature was verified, and further analysis focused on this compound. Size reduction and activation of $LaNi_5$ by mechanical milling was investigated using different milling parameters for the purpose of activating the material for hydrogen absorption.

Because it has been shown that addition of aluminum to $LaNi_5$ resulted in improved hydriding and dehydriding properties, that system was studied further here. In this study, aluminum was added to $LaNi_5$ by mechanical milling. Hydriding properties and elemental compositions of the samples were determined afterwards. The hydrogen absorption rate and capacity were compared to that of $LaNi_5$.

Both $LaNi_5$ and its Al doped derivatives exhibited a reduced rate of hydrogen uptake and a reduced hydrogen capacity in the presence of helium. The effects of coating the samples with either gold-palladium or platinum were investigated. It was observed that coating the samples with Pt reduced the negative effect of He, whereas AuPd coating did not have any effect.

Larger scale studies were done using a continuous U-tube hydride reactor, built and tested for separation of H_2 from a 20:80 H_2:He mixture. The amount of hydrogen retained in the bed was determined and found to be less than that for the batch systems.

I dedicate this work to my family members Baris, Nevin, Taylan and Bilgesu for making me what I am.

ACKNOWLEDGMENTS

I first would like to thank Dr. Michael D. Hampton for providing his endless support, patience and especially encouragement throughout the course of my studies. He was a model research advisor and a friend as well to turn Hydrogen Heaven into a very pleasant work environment. I am also very grateful to Dr. Darlene K. Slattery at the Florida Solar Energy Center, my co-advisor, for her input. The current and past members of the Hydrogen Heaven group are also remembered with appreciation; Mirna, Dr. Lomness, Dorian, Edgar, Irene, Gail, Juliana, Oscar and other fellow students who helped me to find the answers in times of trouble and shared the fun in times of success, thank you very much. The assistance from the all faculty and staff of the UCF Chemistry Department has played a great role, therefore they deserve a big thank you also. I must especially thank Dr. Brooks C. Madsen and Dr. Christian A. Clausen who contributed their unique academic expertise during the course of my education and valuable comments and critiques for my thesis.

Despite the thousands of miles between us, the remarkable morale support I received from my mother Nevin and wise guidance from my father Baris kept me on alert and aware of what could be achieved with ambition and hard working. Thank you a million times.

I also would like to cheer for my friends who supported me indirectly, by giving their understanding and motivating me. Melih, Kemal, Erkan, Atilla, and all the others, thanks a lot.

The members of Tavuk; Aydin, Emre, Emre, Ercan and Ozgur also deserve a big thank you. You are all one of a kind. My friends Havva, Aysun and Banu have been a role model to me with their successes in the academia and they deserve special thanks also. Umut, Erbil, Alper, with you guys we've learned how to learn and, this is irreplaceable.

And last but not least, Kimberly, thank you so much for being there when I needed you. With your loving and caring friendship and a lot more, it has been and is still a joyful journey.

TABLE OF CONTENTS

LIST OF FIGURES

LIST OF TABLES

1. INTRODUCTION

The focus of this study is the separation of hydrogen helium mixtures formed at the Kennedy Space Center (KSC), where hydrogen is used as fuel for the space shuttle main engines, as well as in the fuel cells, and helium is used as the purge gas. The waste purge gas is one of the two different kinds of hydrogen loss at the center. The other is the loss of hydrogen from boil off from the liquid.

A major loss of hydrogen from boil off occurs when liquid hydrogen brought by trucks and rail cars is transferred to storage dewars via insulated pipelines and from storage to the necessary units such as fuel tanks. In this process, loss of hydrogen occurs through

- Cooldown of the vacuum-jacketed lines
- Flash evaporation as high pressure liquid enters the low pressure dewar
- Cooling of the inner skin of the dewar with the rising liquid
- Displacement of the gas above the liquid in the ullage space.

The waste gas is vented to the atmosphere or burned. This boiled off gas is pure hydrogen and its recovery has been studied previously[1].

The flash evaporation of hydrogen as pressure decreases from a tanker transfer pressure of approximately 0.26 MPa (2.57 atm) to a dewar storage pressure of 0.12 MPa (1.18 atm) is the step in the hydrogen transfer that incurs the greatest amount of loss. It is also identified as the most cost effective and readily recoverable loss [2]. It was estimated that 1.5 million gallons (5.68×10^3 m^3) of liquid hydrogen can be recovered. A total of

more than $2 million is projected to be saved annually given that the unit cost of liquid hydrogen is $1.5 gal^{-1} [1].

Apart from pure hydrogen loss, a waste stream containing hydrogen plus helium is also produced. The hydrogen systems and lines are filled with helium when not in service and are purged with hydrogen during loading. Similarly, after usage, the remaining hydrogen is purged out with helium. A total of 2 million standard cubic meters of liquid helium are lost per year [2]. The hydrogen lines and systems are purged with helium because the boiling point of helium is low enough to avoid condensation in the lines. Reliquefaction of hydrogen for reuse is not possible because of the unavailability of economically sized equipment to match the high rate of loss. Furthermore, since the losses are intermittent, the efficiency of the reliquefaction equipment would be low due to down-time. Therefore, a recovery system has to be considered that can effectively separate hydrogen from the mixture, store and redeliver it for reliquefaction.

1.1. Hydrogen Separation And Recovery

Industrial separation of gaseous mixtures has been performed by various approaches depending on the differences in physical or chemical properties of the components. The basis of separation for gas mixtures is generally preferential solubility or difference in sorption potentials in a dense phase. In membrane separation, which is a very common gas separation method, the separating agent is a dense phase membrane. It preferentially dissolves and facilitates the transport of one or more of the components

because of the difference in partial pressure of gas components on the two sides of the membrane [3]. Similarly, in absorption processes the difference in solubility is the basis of successful separation where a solvent preferentially dissolves one of the components [4].

The recovery of H_2 or He from their mixtures is not a common task and has not been investigated in detail. Existing studies that most commonly employ membrane technologies, involve mixtures of hydrogen with gases other than helium. Successful systems for separating hydrogen from methane or carbon dioxide at high temperatures (450-900 ºC) in La_2NiO_4-zeolite membrane reactors are reported [5, 6]. Metals, alloys and intermetallics are also used as H_2 selective membranes due to the high solubility of H_2 in these materials that arises from the smaller size of H_2. However, because H_2 and He are so similar in size, most membranes have very close permeances for this gas pair [7]. For H_2 and He mixtures, the reported separation factor using a polymeric membrane is 4.4 at 308 K, where the separation factor is the ratio of the compositions in the enriched stream relative to the ratio in the depleted stream [8]. A separation factor of 4.4 is a relatively low ratio compared to other gas pairs of hydrogen. Therefore, membrane separation of H_2-He mixtures is not an efficient solution.

Materials such as graphite nanofibers, fullerenes, nanotubes, and hydrides that are utilized for hydrogen storage and reversible sorption of hydrogen have potential for application to the H/He separation processes. Nanofibers are reported to absorb hydrogen to 0.6% w/w at most. Fullerenes have high reversible sorption capacities of 7.7% but their use requires large engineering difficulties. These difficulties include high pressure of activation (500-800 atm) and high operation temperatures of around 500 ºC [9].

Hydrides, on the other hand, provide alternatives with less rigorous operational requirements and with enhanced safety and cost efficiency. They have previously been the subject of investigation for the recovery of pure hydrogen boil-off [2].

1.2. Metal Hydrides

1.2.1. Formation of Hydrides

The unique electronic structure of hydrogen with one electron in the 1s orbital allows it to interact and form compounds with most of the elements in the periodic table. The chemical combination of hydrogen with most metals and metalloids leads to the class of compounds known as metal hydrides [10]. The small size of hydrogen versus other atoms results in relatively faster diffusion in the metal matrix especially below 300 ºC, yielding perceptible concentration changes within short times. Room temperature hydriding occurring at practical rates opened the way to low temperature hydride studies that started in the early 1960s and accelerated along with the advent of the hydrogen economy concept during the following decade [11].

A metal-hydrogen system can be exothermal or endothermal depending on the direction of heat flow during reaction. Endothermal systems show very limited hydrogen solubility and they form no hydrides. On the other hand, the hydrogen systems of the alkali and alkaline earth metals and the transition metals of group 7 to group 8 of the periodic table including palladium systems are exothermal. These are capable of forming

hydrides by dissolving large amounts of hydrogen. All phases of metal-hydrogen systems other than random interstitial solid solutions are designated as hydrides [12]. Depending on the nature of the metal-hydrogen bond, hydrides are classified into three types: covalent, ionic or metallic hydrides. Covalent and ionic hydrides have non-metallic character whereas metallic hydrides preserve the metallic properties of the original metal or alloy.

The solution reaction predecessor to hydride formation is described by five partial steps:

1. H_2 (g, bulk) $\rightleftarrows$ H_2 (g, gas-solid interface)
2. H_2 (g, interface) $\rightleftarrows$ H_2 (physisorbed on metal M)
3. H_2 (phys) $\rightleftarrows$ 2 H (chemisorbed on M)
4. H (chem.) $\rightleftarrows$ H (dissolved in M, solid solution α-phase)
5. diffusion of H in M

In the case of adherent hydride layer formation at the metal-gas interface, additional reaction steps are involved [13];

6. diffusion of H through the MH_x layer
7. M + x H (in MH_x) $\rightleftarrows$ MH_x (β-phase)

When the concentration of hydrogen atoms in the α-phase (solid solution phase) exceeds the solubility limit at the given temperature, β-phase (hydride) is formed. Hydrogen dissolution and hydride formation are physical and chemical processes, respectively.

Any of the surface processes or bulk diffusion in the hydride phase can be the rate determining step in hydriding. Since the hydrogen uptake experiments will depend on too many non-intrinsic parameters, such as the morphological characterization, heat transfer or system configuration; meaningful basic information on the microscopic mechanisms controlling the reaction can not be deductible in this study [14].

1.2.2. Characterization of Metal Hydrides

Virgin metal surfaces are almost never free of a thin oxide layer. That layer limits the interaction of H_2 with the metal under that layer. However, in the initial stages of interaction with H_2, the parent metal or alloy surface cracks from the internal stress caused by the expansion of the crystal lattice from hydrogen insertion. This exposes clean metal surfaces to hydrogen [15]. This makes the initial formation of a metal hydride a kinetically auto-catalytic reaction [16]. After decomposition and release of H_2, the metal is left with a higher surface area relative to its original state. Consequently, with at least one hydriding/dehydriding cycle, the metal is now considered activated and can absorb hydrogen at lower temperatures and pressures and at a faster rate.

The composition of a hydride, $\boldsymbol{c}$ can be expressed as the ratio of the number of hydrogen atoms to the number of atoms of hydride forming metal or alloy atoms (H/M). The relationship of x with pressure, p, and temperature, T, is obtained from pressure-composition isotherms. These isotherms give information about the equilibrium pressure of hydrogen over a metal sample at a given temperature. At a given temperature, a

hydrogen storage alloy has a specific equilibrium pressure of hydrogen (P_{eq}). At low concentrations all isotherms have a common slope showing the relation

$$c \propto \sqrt{p}$$

The hydrogen solubility shows a thermal-activation type of behavior, and the overall expression of solubility takes the form [12]

$$c = \sqrt{\frac{p}{p_0}} e^{\Delta S_s / k} e^{-\Delta H_s / kT}$$

where ΔS_s is the entropy and ΔH_s is the enthalpy of solution at temperature T referring to the H_2 gas pressure p_0. The relationship is often written in the form $\sqrt{p} = K_s c$, where K_s is called the Sievert's constant. The values of K_s have been experimentally determined and reported for most hydrides. The *p*-*c* diagram of $LaNi_5$ is given in Figure 1 as an example.

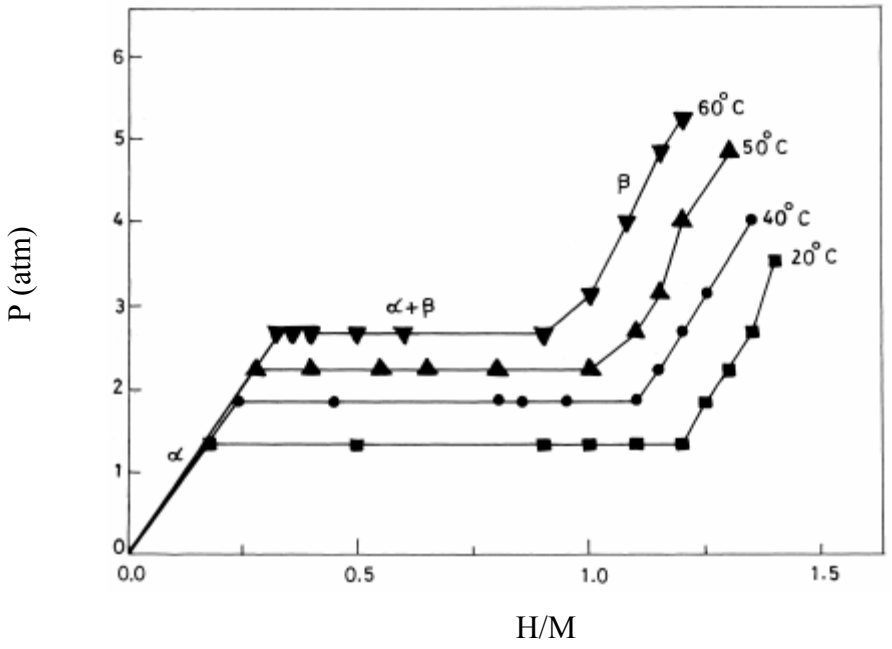

Figure 1. Pressure-composition diagram for $LaNi_5$ [17].

The existing phases and their compositions for different pressures and temperatures are represented in the diagram. With the initial introduction of hydrogen to the metal, the solid solution phase (α) is formed. As pressure is increased, the α-phase becomes saturated with H, after which the hydride phase (β) starts to form. In the plateau region, both phases co-exist. At H/M ratios high enough to correspond to the completion of α to β conversion, only β-phase exists.

Hysteresis is a phenomenon that is commonly observed in metal-hydrogen systems. It is the observation of lower decomposition plateau pressure compared to formation plateau pressure. Hysteresis is not a desired property for practical applications and should be considered when designing an application. Despite the many publications about the degree of hysteresis in specific systems, it is risky to use these data for hydride device design because hysteresis is not a unique materials property and is dependent on history of the sample and the test method used [18].

Other problems, such as heat transfer, may arise when scaling up a hydride system. In that case, heat must be provided to decompose these compounds and release the hydrogen, while heat is liberated when the compounds are formed and must be removed to allow the hydriding reactions to proceed to completion [19].

The desired characteristics of hydrides for practical applications are [18]

- High hydrogen capacity
- Moderate hydriding temperature and pressure
- Moderate dehydriding temperature
- High rate of hydriding
- Low susceptibility to capacity loss by cycling

- Insensitivity to poisoning by impurities
- Low manufacturing costs

Hydride formers usually do not possess the above characteristics in their pure form. Nevertheless, hydride formers can be improved by various methods, such as the addition of one or more new elements to form alloys or intermetallic compounds, changing the sample preparation method, applying activation procedures, or employing protective/catalytic surface treatment. For example, alloying is a common method to decrease the stability of hydrides of pure metals so that hydrogen is recoverable at moderate temperatures [20].

Combining different metals can form either alloys or intermetallic compounds. Alloys are physical mixtures; however, intermetallics (AB_x) are compounds. Intermetallics are composed of an intermediate phase between A and B with different structure from both the parent elements and the terminal solid solutions. Within the domain of homogeneity of an intermetallic, various structural defects and antiphase boundaries might exist. In an intermetallic system, experimental reproducibility is harder to attain and impurities may play a greater role in effecting the stability of the phase, compared to elemental materials, since they are not well defined materials. Impurities may play an important role in the degree of shift of composition between the surface layers and the bulk [21]. Generally the properties of intermetallic compound hydrides have little or no resemblance to those of the constituent metal hydrides [22].

1.2.3. Examples of Hydrides

The formation of Mg_2NiH_4, a covalent hydride of the typical Mg-based intermetallic compound Mg_2Ni, was first published in 1968. The reported initial hydrogen capacity was 3.6% at 598 K and 20 atm of pressure. However activation of the samples after several hydriding/dehydriding cycles, the reaction onset temperature and pressure dropped to 473 K and 13.6 atm [23]. Subsequently, the activation temperature was reduced to 413 K and 404 K by treating the surface with water [24] and water vapor [25], respectively. Other than surface treatment, attempts to control the reaction temperature by simultaneous substitution did not succeed in lowering the dehydrogenation temperature significantly [26].

In the early 1970's, the intermetallic compound $LaNi_5$ was reported to react with H_2 at room temperature to form $LaNi_5H_{6.7}$ which contains 1.53% hydrogen [16]. Processes of both absorption and desorption of hydrogen in this alloy were reported to be rapid at and above room temperature [27] and adsorption or desorption rates were reported to have no dependence on pressure below 5 atm [28].

Vanadium-titanium based alloys, V-Ti-X (X=Fe, Mn, Co, Ni, etc.) were prepared and tested starting from the early 1980's [11]. Out of the 26 alloys tested [29] $Ti_{43.2}V_{49.0}Fe_{7.5}$ was reported to absorb hydrogen up to 3.9% at 253 K. However, the recoverable capacity was 2.4% for absorption at 253 K and desorption at 573 K at 1 atm H_2 pressure. The difference in the absorbed amount and capacity occurs because not all of the hydrogen is desorbed at this temperature. Another Ti-Mg-Ni alloy prepared by ball milling has been shown to absorb 11% hydrogen at 365 K [30]. However, the 11%

hydrogen capacity was not reproducible due to commercial unavailability of manufacturing equipment supplies.

Zirconium based alloy ZrCo was reported to absorb less than 0.1% hydrogen at 473 K [31]. ZrNi was reported to absorb approximately 3% hydrogen at room temperature, with a considerable hysteresis during desorption, and the reaction between ZrNi and H_2 was completed in more than 55 hours [32]. Zr_3Al_2, ZrV_2 and ZrNi particle beds were reported to rapidly and selectively remove hydrogen from a hydrogen/argon stream, eventually reducing the hydrogen content from 10% to 1 ppm by low temperature H_2 adsorption [19].

1.3. $LaNi_5$

After a review of several the candidate materials, Mg_2Ni, VTiNi and $LaNi_5$ were selected for study. Emphasis was placed on $LaNi_5$, as will be discussed in this thesis. It was selected because it exhibits excellent properties for use in a successful hydrogen recovery-storage-delivery system [2]. $LaNi_5$ rapidly reaches equilibrium with hydrogen, even at low pressures and temperatures. Also, the hydriding and dehydriding processes are reversible at H_2 partial pressures close to atmospheric [28]. $LaNi_5$ exhibits low hysteresis and is not strongly affected by gaseous impurities or by oxidation. On compounds such as Nb, V, Ta, FeTi, oxidation creates a barrier for the interaction and dissociation of H_2 molecules. On the surface of $LaNi_5$, the highly reactive La reacts with

oxygen, keeping Ni metallic and, thus, available for the dissociation of H_2 molecules [33].

Methods to improve the hydrogenation properties of $LaNi_5$ included substitution of other elements for either La or Ni, surface treatments, or changing the sample preparation methods. $LaNi_5$, and its substituted derivatives, have found technical applications for hydrogen purification, heat pumps and, most successfully, electrochemical energy storage that replaced Ni-Cd batteries. $LaNi_5$ and derivatives are investigated for electric vehicles because of their higher capacity and lower toxicity.

Substitution of La by other rare earth elements or transition metals has been reported to deteriorate the hydrogen absorption properties [34]. Partial replacement of La by cerium (Ce), praseodymium (Pr), and neodymium (Nd) has been studied to overcome the effect of oxidation in $LaNi_5$ based alloy electrodes; however, H_2 uptake from the gaseous state has not been studied [35].

Partial replacement of Ni with Al, Sn, Ge, Zn, Zr, etc. has been reported to have positive effects on plateau pressure due to larger atomic radii of the substituting elements. Generally, such substitution decreases the hydrogen equilibrium pressure and slightly decreases hydrogen capacity. This is due to an increased heat of reaction (ΔH_{rxn}) and increased unit cell volume, even with small amounts of Sn [36]. Substitution of Ni with germanium (Ge) [37] or zinc (Zn) showed similar results [38].

Substitution of La by Zr and partial substation of Ni with Co resulted in a decrease in hydrogen capacity. However, the lack of a plateau region in the p-c-T diagram indicated the absence of a hydride phase, which means the hydride formed was an interstitial solid solution [34]. Aluminum (Al) partially substituted for Ni in $LaNi_5$

showed the lowest plateau pressure and the highest cell volume among $LaCo_5$, $LaNi_5$, $LaCo_2Ni_3$ and several other compounds. As the extent of substitution increases, the cell volume expansion was greater [39]. Al was found to increase the cycle lifetime without significantly decreasing in hydrogen capacity. For $LaNi_{4.5}Al_{0.5}$ and $LaNi_4Al$, the heat of formation of the hydride (ΔH) was found to be more exothermic by -38 and -46 kJ per mole, respectively [40]. In another study, increasing Al content was reported to have an adverse effect on the hydrogen capacity of $LaNi_{5-x}Al_x$ (x=0 to 0.5) prepared by arc melting, followed by crushing [41].

One of the problems associated with the use of $LaNi_5$ for hydrogen storage is disproportionation upon cycling. The desired reversible reaction

$$LaNi_5 + 3\ H_2 \rightleftarrows LaNi_5H_6$$

is actually thermodynamically unfavorable relative to the less reversible disproportionation reaction

$$LaNi_5 + H_2 \rightarrow LaH_2 + 5Ni$$

The disproportionation reaction requires the diffusion of metal atoms, which is a slow process at low temperature, and thus, the hydrogen desorption reaction predominates near room temperature [18, 42]. Despite the detectable disproportionation with extended cycling, good engineering lives were achieved for $LaNi_{4.7}Al_{0.3}$, which showed less than 5% H capacity loss after 1500 cycles at 85 ºC. The hydrogen capacity loss was 25% for $LaNi_5$. It was found that the structural disintegration is reversible by heating the sample to 300 ºC for about 4 hours under vacuum to remove all bound hydrogen and reform $LaNi_5$. The hydrogen capacity was completely restored to its original value by this process [43].

1.4. Mechanical Alloying

Preparation of intermetallics and alloys on the laboratory scale is possible by melting, annealing or mechanical alloying, or a combination of several techniques [21]. The alloys studied in the literature were prepared by arc melting of the stoichiometric amounts of pure elements. Those samples were reported to be analyzed without significant size reduction, i.e. as large pieces, except where indicated.

An alternative to the fabrication of alloys and intermetallics by arc melting is mechanical alloying. This solid state powder processing technique involves repeated welding, fracture, re-welding, and mixing of a blend of elemental or pre-alloyed powders in a ball mill [44]. Ball milling can result in both equilibrium and non-equilibrium states, size reduction, chemical reactions, and possible phase changes. The metastable non-equilibrium state formed by "energizing and quenching" is a phase between equilibrium crystalline and an energized state in solid, liquid or vapor form (Figure 2). Energizing the material is bringing it to a highly non-equilibrium state by an external force such as melting, evaporation, irradiation, pressure application, or storing of mechanical energy by plastic deformation. Mechanical alloying/milling introduces energy into the milled material and this energy is stored as atomic disorder and/or grain boundaries which can be represented as

$$\Delta G_{\text{milling}} = \Delta G_{\text{disorder}} + \Delta G_{\text{grain boundaries}}$$

Mechanical alloying is reported to introduce a significant amount of stress, chemical disorder, and defects to the material [45]. Since hydride formation occurs at the incoherent sites such as dislocations [46] and internal interfaces [47], the formation of

grain boundaries increases the total hydrogen affinity of the material. Another effect of milling is the removal of the oxidized surface layers that create a barrier for hydrogen absorption. During milling in an inert atmosphere, active fresh metal surfaces are created, which will readily dissociate H_2 upon exposure. Thus, after activation by mechanical milling, a material can readily react with hydrogen [46]. One important feature of ball milling is that it allows the production of alloys from elements with high vapor pressure or poor miscibility [48].

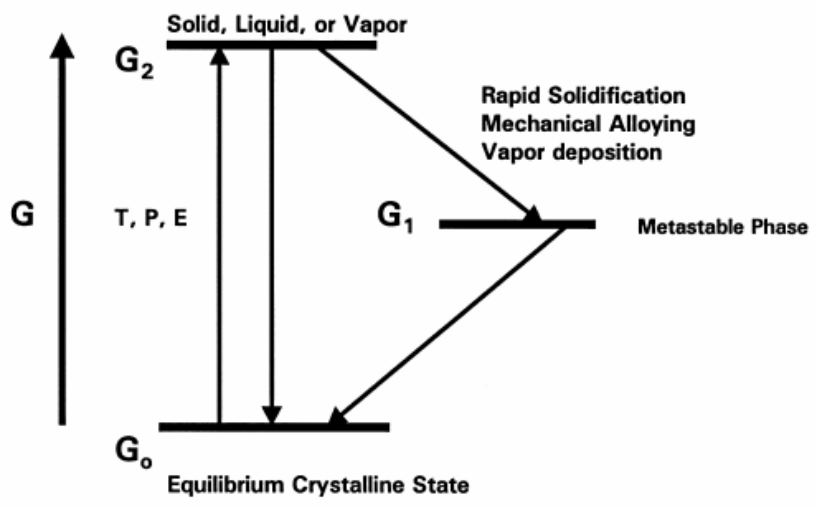

Figure 2. Energy diagram for metastable phase formation by mechanical alloying.

The phase and/or microstructure of a material after milling depend on several variables. These are listed below along with their influences on the final product.

- *Type of mill* is chosen according to the needed quantity of product, speed of milling, and final constitution.
- *Milling container* shape is generally dictated by the type of mill; however flat or round ended vials might be available.
- *Milling speed* has direct effect on the energy input to the powder.
- *Milling time* is chosen so to achieve a steady state between fracturing and cold welding of the particles.
- *Type, size and distribution of the grinding medium* are determined by the type of mill and influences the time of milling.
- *Ball-to-powder weight ratio* is effective on the successful impacts on the powder by the balls and is decisive in time of milling.
- *Extent of filling the vial* is critical as small quantities of balls and powder will not have good production rates. On the other hand, filling the vial too much will not leave enough space for the balls to move around, thus, reducing the energy of impact.
- *Milling atmosphere* highly effects contamination of the powder and the product. Therefore, vials are either evacuated or filled with an inert gas such as argon or helium. If an interaction is desired with a gaseous reactant, then the vial is filled with that gas.
- *Process control agents,* usually organic surfactants, can be used to reduce the effect of cold welding.
- Temperature of milling is effective on diffusion processes during alloying and may also influence the brittleness of the powder.

These parameters are generally interdependent. For example, the optimum milling time is affected by the type of mill, temperature, etc. Ball to powder ratio (BPR) and time of milling for a desired product are dependent on the capacity of the mill. For small capacity mills, BPR of 10:1 is reported to be the commonly used [47].

Ball milling has been reported to activate FeTi, Mg_2Ni and $LaNi_5$, which are inert to hydrogen prior to milling. For FeTi, milling is believed to give rise to Fe rich clusters on the surface and the generation of new surfaces by cracking [49]. $LaNi_5$ has been synthesized from elemental La and Ni via milling at room temperature and, using a similar method, the partially substituted $La_{0.5}Zr_{0.5}Ni_5$ has been synthesized from an equimolar mixture of $LaNi_5$ and $ZrNi_5$ [48].

1.5. Crystallography Of Hydrides

The understanding of the crystallographic aspect of hydrides and their precursors is important in terms of materials characterization. The positions of the host metal before, during and after hydride formation have been reported. The orientation of hydrogen within the material and the physical and chemical changes experienced by it has been investigated to justify the limits of hydriding reactions from a structural point of view. These parameters affect phase changes and physical properties, and change with composition or outside conditions. Therefore material characterization is a necessity for each different sample under study.

Atoms in crystalline solids are at the points of intersection of a network of lines in three dimensions that is called a space lattice. Each point in the lattice has identical surroundings so each lattice can be described by specifying the atom positions in a repeating unit cell. The unit cell is described by three lattice vectors originating from one corner of the cell. The axial lengths a, b and c and the interaxial angles α, β and γ are the lattice constants of the unit cell. The space lattice of an ideal crystalline solid and the unit cell showing lattice constants, is given in Figure 3.

Seven different types of unit cells are required to create all point lattices and 14 standard unit cells can describe all possible lattice networks. For example, $LaNi_5$ has a hexagonal unit cell with $CaCu_5$ type structure given in Figure 4. For a hexagonal unit cell, two of the axes are at 120º and the third axis is at a right angle to the first two where $a = b \neq c$, $\alpha = \beta = 90º$, $\gamma = 120$ º.

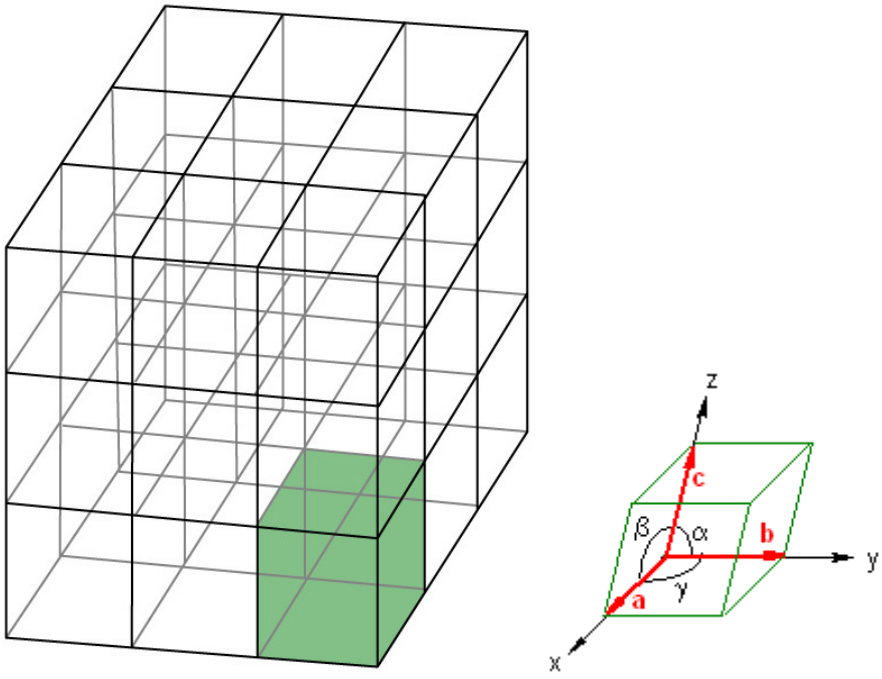

Figure 3. Cubic space lattice of an ideal crystalline (left) solid and the unit cell (right) [50].

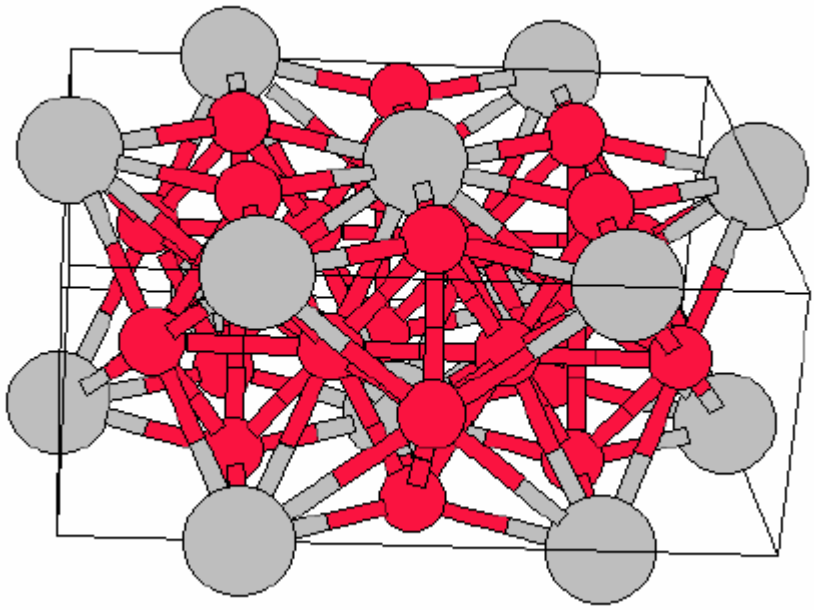

Figure 4. CaCu5-type P6/mmm structure of $LaNi_5$ [51]. Gray spheres indicate La atoms.

Pure metals and alloys usually have simple crystal structures like body centered cubic, face centered cubic or hexagonal close packed structures. Hydrogen atoms usually occupy either tetrahedral or octahedral interstices in those structures [52]. Interstitial sites occupied by hydrogen in the host lattice result in expansion of the crystal lattice. Each hydrogen interstitial causes displacements of the metal atoms from their regular sites and the resulting crystal lattice distortions cause physical property changes. Volume expansions of 20% are typical for the solution of one hydrogen atom per metal atom [52]. This phenomenon is responsible for the lower terminal H solubility in block samples of $LaNi_5$, compared to powder samples, because of the limited expansibility of block samples with larger crystal grains as opposed to the ready stress relaxation of smaller particles [53].

One of the limiting factors for hydrogen storage capacity and uptake rate is the reluctance of hydrogen to occupy all available interstices in the metal atom network; thus, detailed structural data are needed, if possible, to understand this phenomenon [54]. Mostly, the determination of hydrogen positions has been accomplished by neutron vibrational spectroscopy [54-56], which is not considered in this study.

The addition of different elements also affects the crystal structure. There are different types of imperfections in crystalline structures. A vacancy is a point defect, which is the absence of an atom from an atomic site. Dislocations are line defects that cause lattice distortion centered around a line [57].

In the case of $LaNi_5$, lattice constants are reported to increase with the addition of Al [40] and crystalline imperfections occur. With the substitution of Ni with Al, the dislocation density and vacancy concentration induced by hydrogenation are reported to decrease [58].

In another study, mechanically alloyed $LaNi_{4.2}Al_{0.8}$ (from its corresponding pure elements milled for 30 hours in a Spex 8000 Mixer Mill using a round bottom stainless steel vial) was reported to form an amorphous phase directly from the starting mixture without formation of another phase. The $La(Ni,Al)_5$ alloy with a hexagonal $CaCu_5$ phase was formed only after annealing at 750 ºC for 0.5 hour [59]. For the samples prepared with that sequence, the surface segregation of La was more pronounced than that of polycrystalline powders from arc-melted ingots. Thus, an increment in solid state solubility was observed [60]. This was explained by the increased area of Ni clusters, which play an important role in the adsorption of H_2 to the surface.

In this study, the addition of Al to the $LaNi_5$ system was performed by mechanically alloying the $LaNi_5$ with Al using a flat bottom tungsten carbide vial in a Spex 8000 Mixer Mill. The mole percent of Al in $LaNi_5$ was varied from 0.87% to 48.57% corresponding to $LaNi_5Al_{0.05 \rightarrow 5.67}$.

$LaNi_5$ itself has been previously verified to be potentially used at the Kennedy Space Center for recovery of boil-off hydrogen [61]. The main objective of the study described in this thesis was the evaluation of $LaNi_5$ and $LaNi_5Al_x$ for the separation of H_2 from its mixtures with He. First, hydrogen uptake capacity and rates of the materials from pure H_2 were determined and compared to the published results. Then behavior of the materials when exposed to a mixture of H_2 and He at different pressures was determined using the same experimental setup and presented. The amount and state of Al in the samples were correlated to the H_2 uptake capacity and rates, for both pure H_2 and H_2-He mixtures.

To improve the behavior of $LaNi_5$ and $LaNi_5Al_x$ with H_2-He mixtures, the samples were coated with AuPd, which is known to be very permeable to hydrogen. These sampes were analyzed with the same procedure and the results are described in section 3.2.2.4.

The materials were characterized using X-ray diffractometry, which gave information about crystal structure and formation of new compounds by ball milling. Due to the possibility of segregation of elements during ball milling and sticking permanently on the milling media, the elemental composition of the samples was not expected to be the same before and after ball milling. Therefore, it was crucial to determine the exact

composition that was responsible for the results obtained in the H_2 uptake analysis. The compositional analysis was done by flame emission spectrophotometry.

2. EXPERIMENTAL

2.1.Chemicals and Reagents

Lanthanum nickel, $LaNi_5$, was purchased from two different sources, -35 mesh Hy-Stor 205 Alloy was purchased from Ergenics Inc. and Reacton (99.9%) was purchased from Alfa Aesar. Aluminum (99.5%, -325 mesh), vanadium (99.5%, -325 mesh), titanium (99.5%, -200 mesh), and nickel (99.9%, -100+200 mesh) were acquired from Alfa Aesar. Magnesium nickel alloy, HY-STOR 301, was obtained from Aldrich. Lanthanum(III)oxide (99.99%) was obtained from Acros Organics. High purity grade hydrogen, high purity grade helium and ultra high purity grade argon were purchased from Air Products. Hydrogen-helium mixtures of 50% and 20% (v/v) hydrogen in helium were obtained from Air Liquide.

2.2. Equipment and Instrumentation

All materials to be ball milled, analyzed in a SETARAM DSC 111, or analyzed in the U-tube reactor were loaded into a vial, sample boat, or reactor in the argon atmosphere of a Labconco Protector Controlled Atmosphere glove box with an Atmospure gas purifier.

For the ball milling of lanthanum nickel, vanadium titanium nickel, magnesium nickel, and lanthanum nickel aluminum alloys, a high energy Spex 8000M Mixer/Mill was used, Figure 5. Small samples were prepared using a 50-mL tungsten carbide grinding vial obtained from Spex Certi Prep Inc., Metuchen, NJ, was used with two 11.11 mm tungsten carbide balls as the high energy ball milling medium. Other samples were prepared using a 50-mL stainless steel grinding vial with 12.70 mm stainless steel balls obtained from the same company. These samples were previously prepared by other researchers in our group to be used in the U-tube and Parr reactors.

In addition to the Spex 8000 Mixer Mill, a Fritsch Pulverisette 6 Planetary Mono Mill was also used for the ball milling of numerous lanthanum nickel samples for DSC analysis, Figure 5. A 250-mL stainless steel grinding vial with 9.7 mm diameter stainless steel balls obtained from Gilson Co., OH was used as the grinding medium.

Figure 5. The high energy Spex 8000M Mixer/Mill (left) and the Fritsch Planetary Mill (right).

2.2.1. Differential Scanning Calorimetry (DSC)

Hydriding and dehydriding characteristics of sample materials were determined using a SETARAM DSC 111 differential scanning calorimeter (DSC). The DSC furnace was fitted with sample and reference cells made from 1/4" Hastelloy C-22 seamless tubing. The cells were connected to inlet and exit valves with quick disconnects for easy access. The inlet and exit valves were needle and globe valves, respectively. The inlet valves were connected to hydrogen and helium cylinders and the exit valves opened to the atmosphere. All components and fittings were made of 316 stainless steel. Pressure

was monitored with two Omega type px602 pressure transducers with a range up to 13.6 atm. The schematic of the complete setup is given in Figure 6. Pressure data were acquired with a Dell 4200 PC using LabView software using a National Instruments board. Thermal data were directly transferred to the PC from the DSC and analyzed using Setsoft 2000 software. The amount of hydrogen absorbed or released was calculated and graphed using SigmaPlot software. This DSC allowed thermal and pressure measurements to be made under static or flowing conditions at pressures as high as 136 atm and temperatures up to 773 K. Sample boats for the DSC were made from 316 stainless steel. The samples loaded into the boat were placed into a hollow glass tube that was sealed at both ends with plastic caps and then transferred from the glove box to the DSC to prevent exposure of the samples to air. Sample cell volume was determined by a water displacement method. Lateral heat loss compensation curves were previously determined.

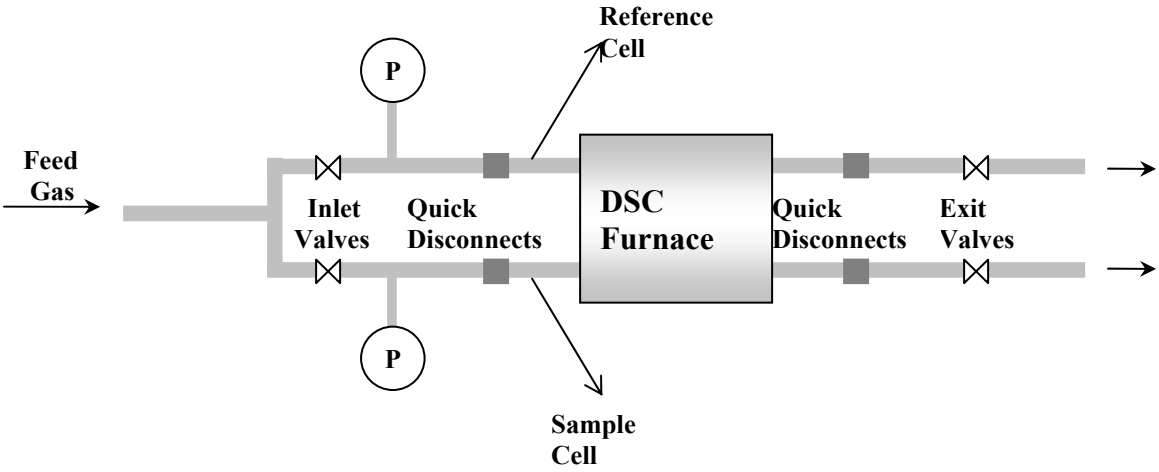

Figure 6. Schematic representation of the DSC setup. P denotes pressure transducer.

2.2.1.1. Hydriding and Dehydriding Procedures

Samples for hydriding trials were prepared by loading 100 to 300 milligrams of sample into sample boats under an argon atmosphere in the glove box. The boats were transferred to the DSC after the furnace temperature had been adjusted to between 10 to 25 °C. The boat was loaded into the cell under a minimal hydrogen flow, which avoided blowing the samples out of the boat and limited air exposure of the samples. After inserting the boat, the exit valves were closed, the system was adjusted to the desired pressure and then the upstream valves and the hydrogen source cylinder valve were closed. The hydriding of the sample was performed either isothermally or with increasing temperature.

Constant temperature hydriding was used for samples that took up hydrogen at ambient or sub-ambient temperatures. In this procedure, pressure and thermal data recording started immediately after the system was closed. The furnace temperature was held constant for the entire experiment period.

Samples that would only hydride at higher temperatures were subjected to the increasing temperature hydriding procedure. After the sample was inserted and the desired pressure over it had been established, the furnace was held at the initial temperature (T_1) for 180 seconds. Then the temperature was increased at a rate of either 5 °C/min or 3 °C/min, up to the previously set final temperature (T_2). The furnace was held at the final temperature for 180 seconds and then cooled at a rate of 10 °C/min, down to ambient temperature. Pressure data acquisition started at the beginning of the heating phase.

The dehydriding procedure was initiated immediately after the system reached ambient temperature at the end of hydriding process. For this procedure, the exit valves were opened to release hydrogen and a minimal argon flow was established using the needle valves. The system was purged with argon for 15 minutes after which the inlet valves were closed followed very quickly by closing the exit valves to maintain atmospheric pressure argon within the system. Dehydriding was accomplished by holding the furnace at the initial temperature for 180 seconds and then heating to T_2 with a ramp rate of 5 °C/min. The furnace was held at T_2 for 180 seconds and then cooled at a rate of 10 °C/min. Dehydriding in a closed system allowed quantization of the H_2 given off by the sample. Hydriding and dehydriding cycles were repeated without removing the sample from the DSC.

Because $LaNi_5$ and $LaNi_5Al_x$ will absorb and release H_2 at ambient temperatures, their dehydriding characteristics were determined using a slightly modified procedure. For these samples, excess H_2 pressure after the hydriding experiment was reduced to 1 atm. Then pressure and thermal data acquisition were started immediately. The system was heated to 150 ºC with no delay period.

2.2.1.2. Thermal Activation Procedure

Some samples were not sufficiently activated by ball milling alone. The activation of these samples was accomplished by a thermal cycle in the DSC following milling. This was done by placing the sample in the DSC in a hydrogen atmosphere at

approximately 5 atm, and heating the furnace to 150 °C, followed by cooling to ambient temperature. During this activation step, samples were hydrided to some extent, if not completely. Therefore, these samples were heated up to 150 °C under a minimal flow of argon to ensure no hydrogen was left in the sample.

2.2.2. U-Tube Reactor

A 1 foot long, 1 inch O.D. seamless stainless steel pipe was bent into a U shape to hold up to 300 grams of sample. The reactor was fitted with 0.5 micron pore size inline filters and needle valves on each end, Figure 7. The compositional analysis of the effluent gas was done by a Buck Scientific type 910 gas chromatograph fitted with a Hayesep DB 100/120, 30 ft, 1/8 inch O.D. stainless steel column obtained from Alltech. The GC utilized a TCD detector and the carrier gas was argon. Samples were taken from a three neck flask connected to the downstream. Sample injection was done with a gas tight 100 μL syringe. The GC was connected to a Dell GX110 PC and the data was recorded using PeakSimple chromatography software.

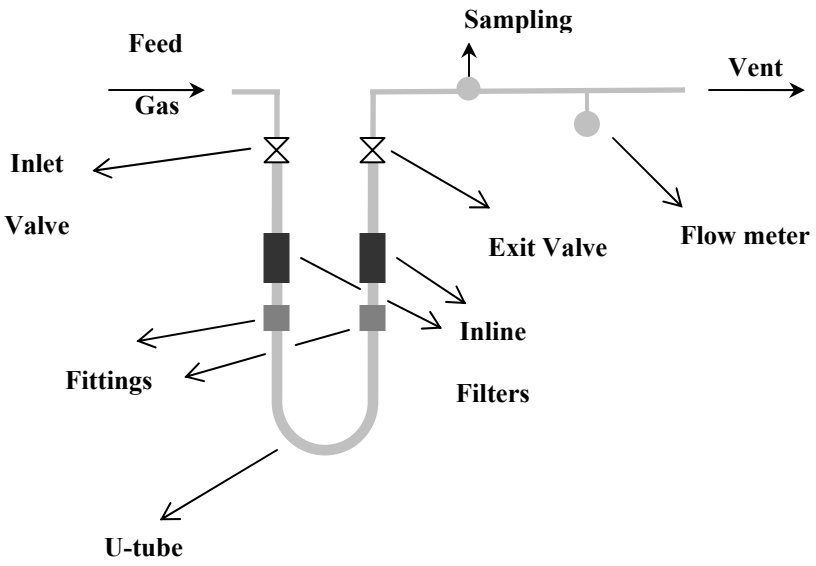

Figure 7. The U-tube reactor.

2.2.2.1. Hydriding and Dehydriding Procedures

The U-tube reactor was used to determine hydriding characteristics via continuous operation. For continuous hydriding, the U-tube was disconnected from the rest of the structure by the quick disconnects and filled with approximately 200 g of sample under argon atmosphere in the glove box. The rest of the structure was then assembled on both ends and the reactor was removed from the glove box. After purging the reactor with argon, a hydrogen/helium mixture was allowed to flow through the reactor. At the same time, samples were injected into the GC continuously with appropriate 1 minute intervals

determined by the start and end of a hydrogen-helium peak pair. The flow rate through the reactor was monitored with a Fisher Scientific digital flowmeter.

Dehydriding of the hydrided samples was accomplished by heating the reactor with heating tape up to 150 ºC under argon flow and analyzing the exit stream for hydrogen using the GC. As soon as no hydrogen was detected in the stream, the heating system was turned off to allow cool down to room temperature for the subsequent experiments.

2.2.2.2. Activation procedure

Samples ball milled in stainless steel vials with lower ball to powder ratios and longer milling times were activated in a high pressure reactor. Approximately 200 grams of milled alloy were placed in a Pyrex Petri dish that was then transferred into a 2000 mL capacity Parr Pressure Reactor. Pressure was monitored with one Omega type px303 pressure transducer with a range up to 34 atm. Temperature in the reactor was regulated by a Love Controls Series 2600 type controller. Pressure and thermal data were acquired with a Dell GX240 PC using Lab View software through a National Instruments board. Samples were heated up to 250 ºC under a hydrogen pressure of approximately 20 atm. After the system reached equilibrium, the heating system was turned off and the system was allowed to cool under hydrogen pressure. After cooling, the system was vented and a heating cycle was run to remove absorbed hydrogen.

2.3. Sample Preparation

$LaNi_5$ and Mg_2Ni samples were prepared by ball milling the alloys. $LaNi_5Al_x$ samples were prepared by milling Al with $LaNi_5$. VTiNi samples were prepared by milling the stoichiometric amounts of V, Ti and Ni. Ball milling was done in either of the mills for $LaNi_5$. For the other materials, the Spex8000 Mixer Mill was used. The milling time was 10, 30 or 90 minutes and the ball to powder ratio was 10 to 1 or 1 to 1. For milling periods greater than 30 minutes, the milling was done in 30 minute periods, followed by 15 minute cool-down periods. Milling was done with 100-300 rpm and 1725 rpm in Fritsch and Spex 8000M mills, respectively. After milling, the vials were opened in the glove box and the samples were first transferred to glass vials for storage, and then portions were loaded in a DSC sample boat.

Some samples were AuPd or Pt coated prior to testing. They were first prepared by ball milling. Coating was done by an Emitech K550 type sputter coater at 20 mA. The thickness of coating was controlled by setting the duration of coating. The dependence of coating thickness on duration of coating had been determined by previous users of the coater, and is given in Figure 8.

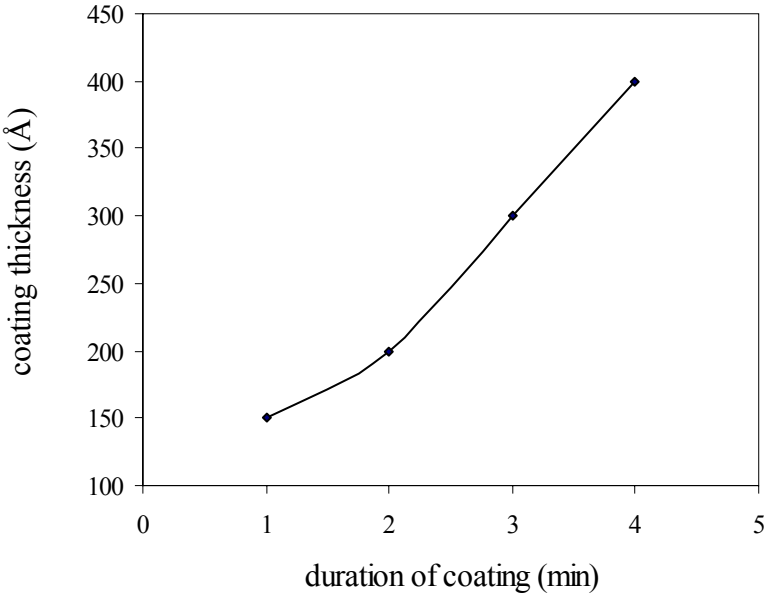

Figure 8. Coating thickness dependence on coating duration.

2.4. Sample characterization and Analysis

A Rigaku Multiflex X-ray diffractometer using Cu Kα radiation, was employed to characterize $LaNi_5$+Al samples. Analysis was done over a 2θ range of 20º to 80º. The slit width and scanning speed were 0.020 mm and 2.400 degrees per minute, respectively. The X-ray generator voltage and current were set to 40 kV and 30 mA, respectively. Samples were supported on a metal sample holder whose bottom was closed by scotch tape and the sample was filled above it. Data were analyzed by Jade analysis software.

Elemental analysis of $LaNi_5$ and Al doped $LaNi_5$ was done by flame emission spectroscopy using a Varian Inc. SpectrAA10 spectrometer. Lanthanum, nickel, and

aluminum were analyzed at 441.7, 341.5 and 396.1 nanometers, respectively. An acetylene/nitrous oxide flame was used with a slit width of 0.2 nm for all elements. Lanthanum standards were prepared by making dilutions from a stock solution of La_2O_3 dissolved in HNO_3. Nickel and aluminum stock solutions were prepared by dissolving pure elements in 1:1 HNO_3 and then standards were prepared by making appropriate dilutions. The interferences of Ni on Al and Al on La were counter balanced by matching the concentrations of the interferences in the standards to that of samples. The interference concentrations were calculated by using the mass and composition of the sample dissolved.

3. RESULTS AND DISCUSSIONS

3.1. Hydride Formers

The small scale testing of hydride forming materials was done in the differential scanning calorimeter (DSC). Hydrogen uptake capacity and onset temperature were determined quantitatively. Qualitative data about the rate of reactions were obtained by observation of the rate of pressure change. The materials selection was based on the literature review, which emphasized factors such as hydrogen capacity, hydriding conditions, as well as safety and availability. The materials subjected to initial experiments were Mg_2Ni, VTiNi, $LaNi_5$ and $LaNi_5Al_x$ where $0.05 < x < 5.67$.

During the course of the experiments, heat flow, in milliwatts, into or out of the DSC sample cell and sample temperature, in ºC, were recorded. The output of the instrument, a thermogram, is a plot of differential heat flow and sample temperature versus time. In this plot, an upward peak represented an exothermic event and named an exotherm; a downward peak represented an endothermic event and is named an endotherm. The design of the pressure cells utilized with the DSC incorporated pressure transducers, and thus, allowed for simultaneous thermal and pressure measurements. The pressure transducer mV output was collected at a sampling rate of one point per second. Then, using the appropriate transform in the SigmaPlot software, the output was converted to pressure in atmospheres and then to percent hydrogen by weight using the number of moles, calculated from the ideal gas law

$$\%H = \frac{m_H}{m_s} = -\frac{\Delta n.AWt}{m_s} = -\frac{\frac{V\Delta P}{RT}.AWt}{m_s}$$

where m_H = mass of hydrogen

m_s = mass of sample

Δn = change in number of moles of hydrogen

AWt = atomic weight of hydrogen atom

V = volume of sample cell

ΔP = change in pressure

R = gas constant

T = temperature

3.1.1. Mg_2Ni

The Mg_2Ni alloy was ball milled and a sample weighing approximately 110 mg was loaded in the DSC and heated up to 250 ºC under 3.7 atm of H_2. The thermogram and the percent hydrogen and pressure curves for the initial hydriding step are given in Figures 9 and 10, respectively. In the thermogram, two exothermic events were observed, of which only the first one is accompanied by a pressure drop. The first peak indicated uptake of hydrogen by the alloy at an onset temperature of 148 ºC. The amount of hydrogen absorbed was slightly less than 3%. The smaller peak observed during cool down was due to some phase change that did not involve absorption or release of gas.

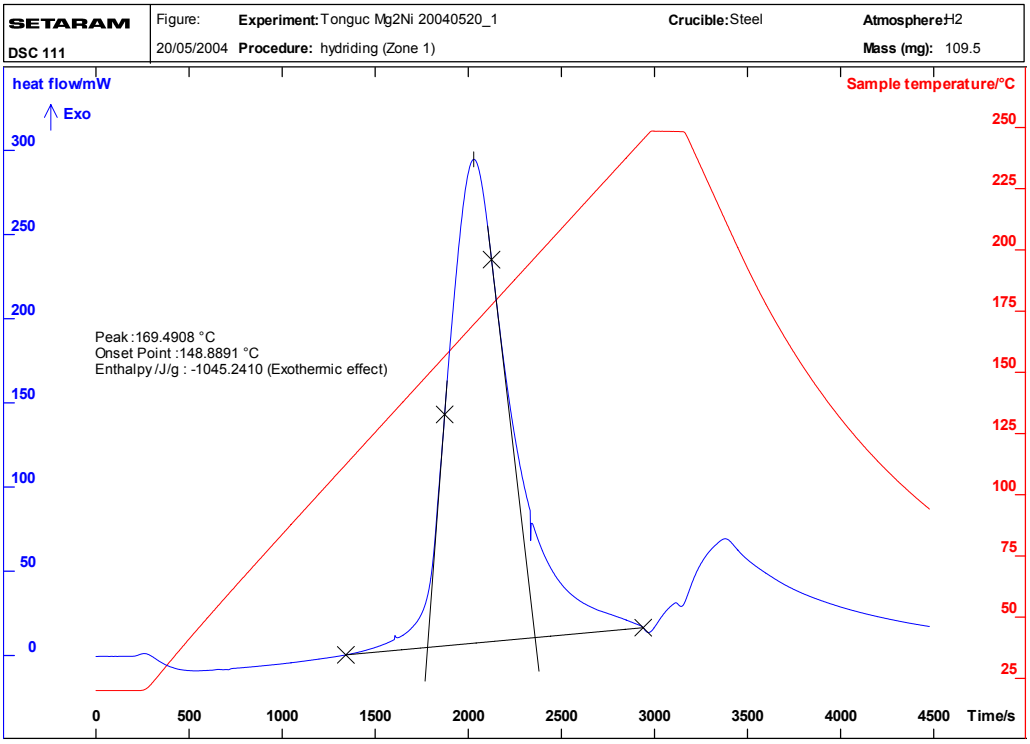

Figure 9: Thermogram for initial hydriding of Mg_2Ni.

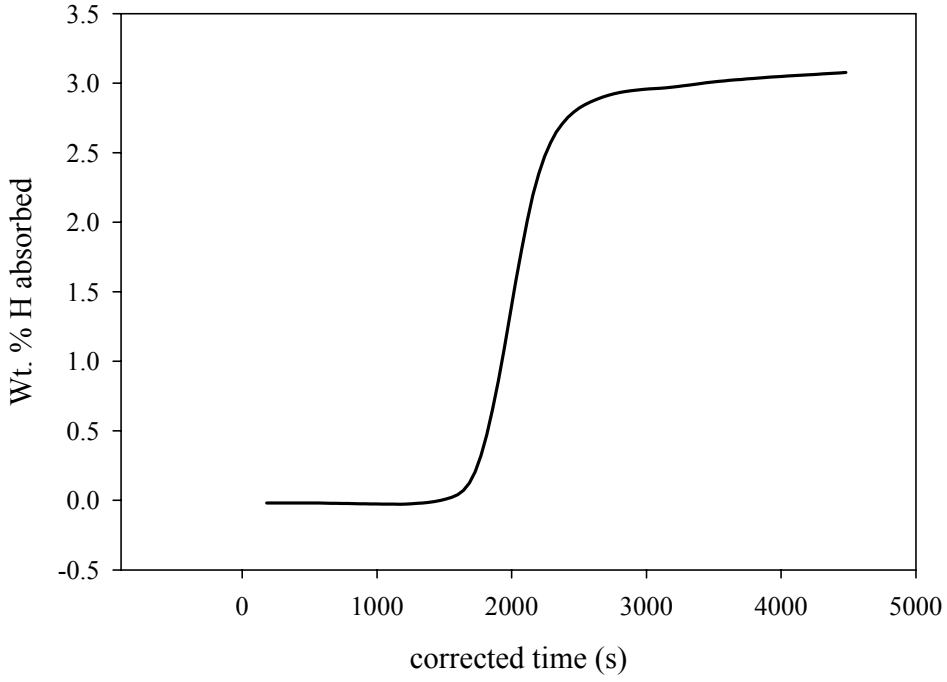

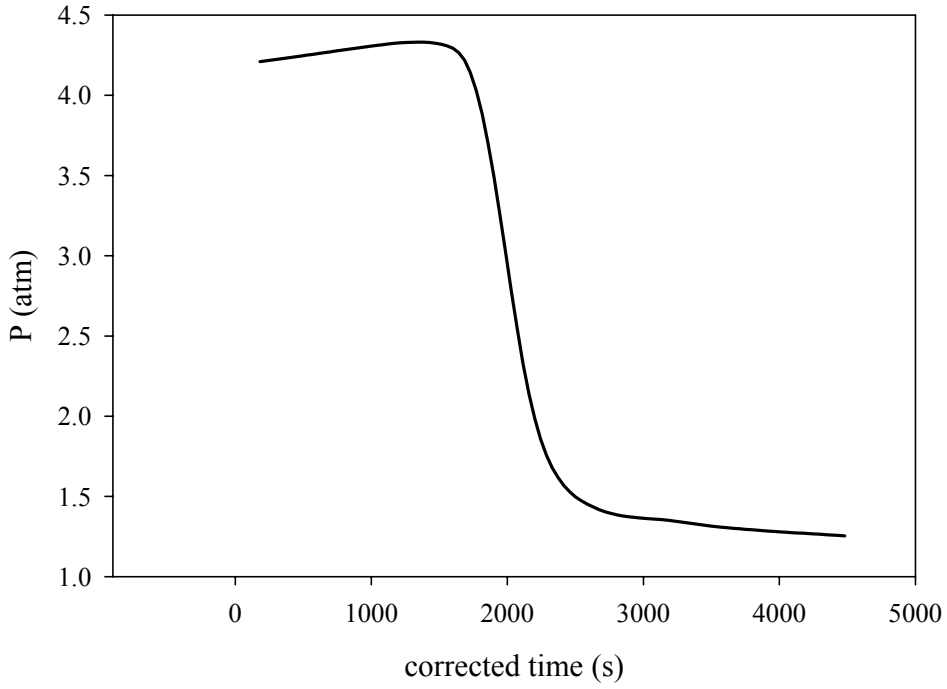

Figure 10: Composition and pressure plots for initial hydriding of Mg_2Ni.

The thermogram associated with the subsequent dehydriding of the alloy exhibited an endothermic event, ascribed to the loss of hydrogen from the alloy, at an onset temperature of approximately 230 ºC. The amount of hydrogen released was limited to 0.15% at 250 ºC, which was not sufficiently hot for complete dehydriding. The sample was dehydrided again and 3% H was released at about 350 ºC. The thermogram and the percent hydrogen desorbed plots are given in Figures 11 and 12. In the thermogram, the endothermic peak is followed by two smaller exotherms. The exotherms are due to the re-absorption of the released hydrogen. This re-absorption occurs as the temperature decreases during the cooldown cycle.

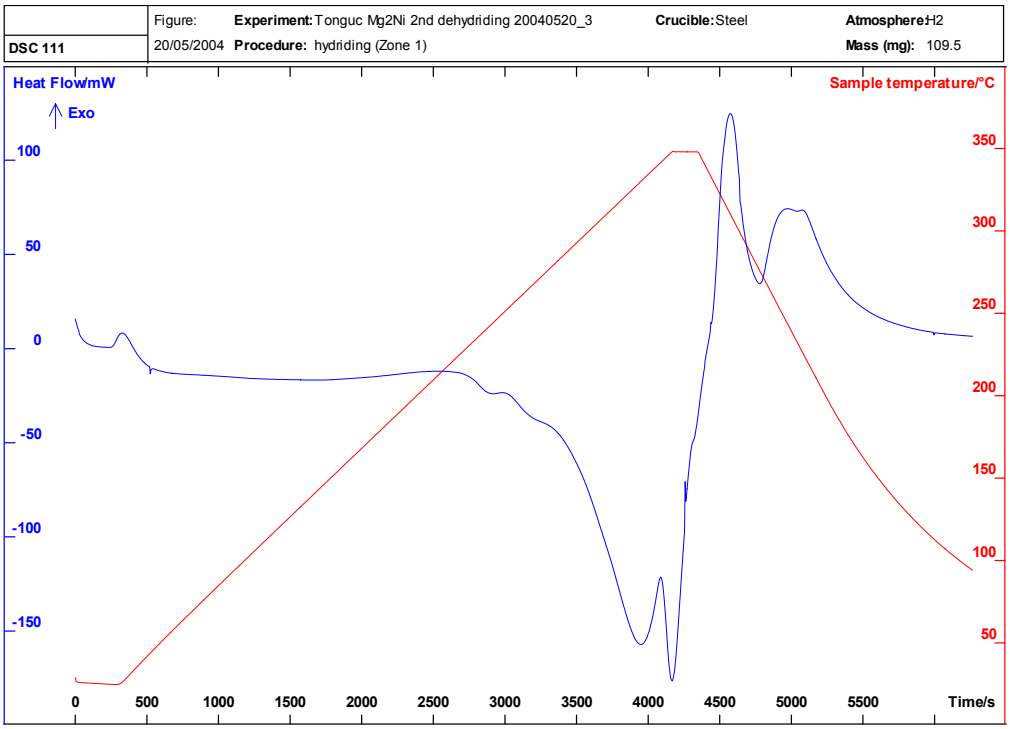

Figure 11: Thermogram for dehydriding of Mg_2Ni.

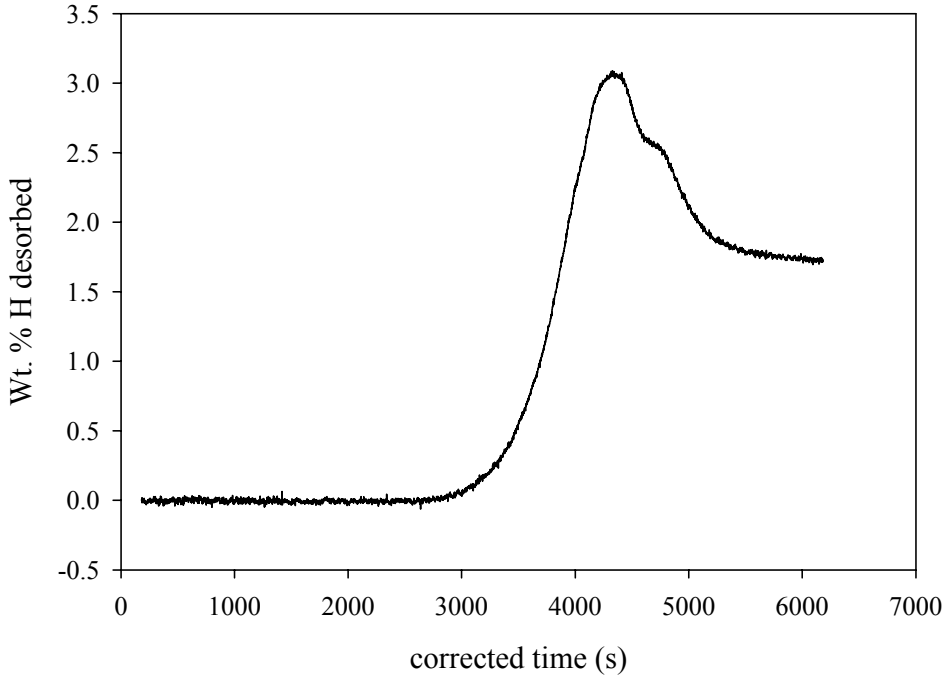

Figure 12: Percent hydrogen desorbed for dehydriding of Mg_2Ni.

Ball milled Mg_2Ni reacted at lower temperatures and H_2 pressures to react than previously reported values [23]. The amount of H absorbed, 3.04 %, ($Mg_2NiH_{3.23}$) was lower than the reported value of 3.60 % (Mg_2NiH_4). The uptake reaction was complete in about 15 minutes.

3.1.2. VTiNi

V, Ti and Ni were alloyed using the Spex8000 Mixer Mill. Since the starting materials were pure elements, a relatively long milling time, 90 minutes, was used. The

total time was broken into three 30 minute intervals separated by two 15 minute cool down periods. The thermogram and composition curve for hydriding of the sample are given in Figures 13 and 14, respectively.

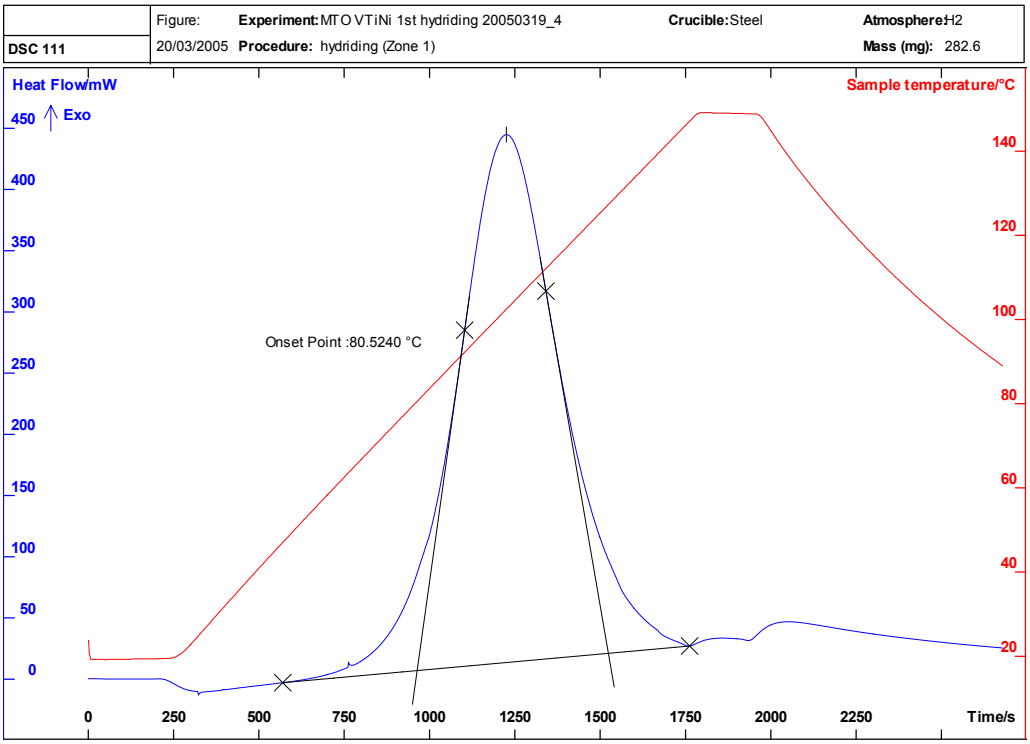

Figure 13: Thermogram for initial hydriding of VTiNi.

After 500 seconds, a drop in pressure started and the accompanying exotherm had an onset temperature of 80 ºC. The terminal H percentage was about 1.1%, corresponding to $VTiNiH_{1.7}$.

Another sample of VTiNi was milled for 10 minutes, a much shorter period. This sample took up approximately 0.6% H at about 90 ºC. This suggested that longer milling times are better for this mixture of metals.

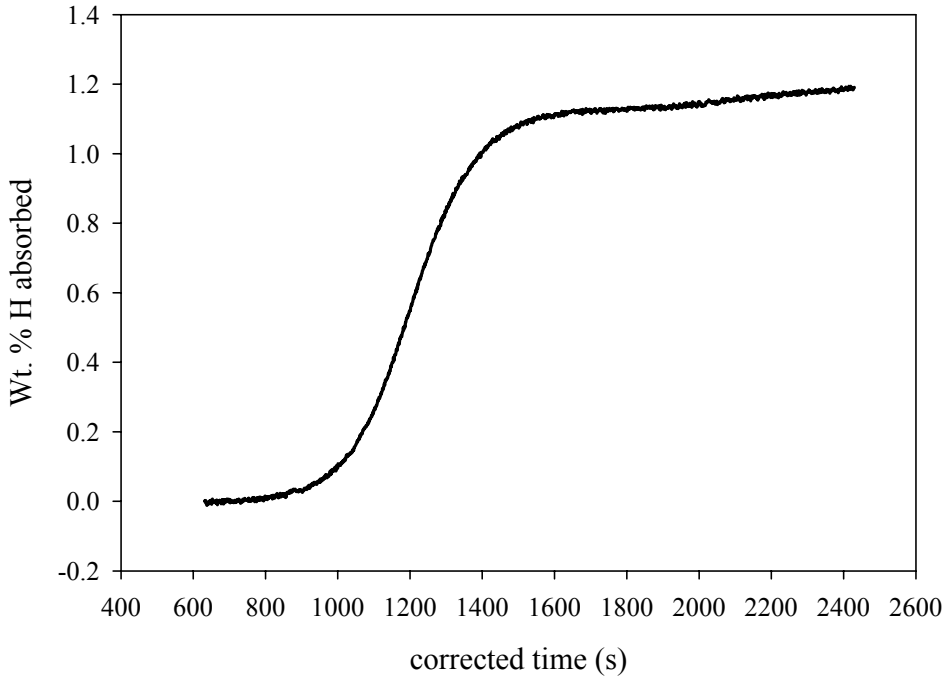

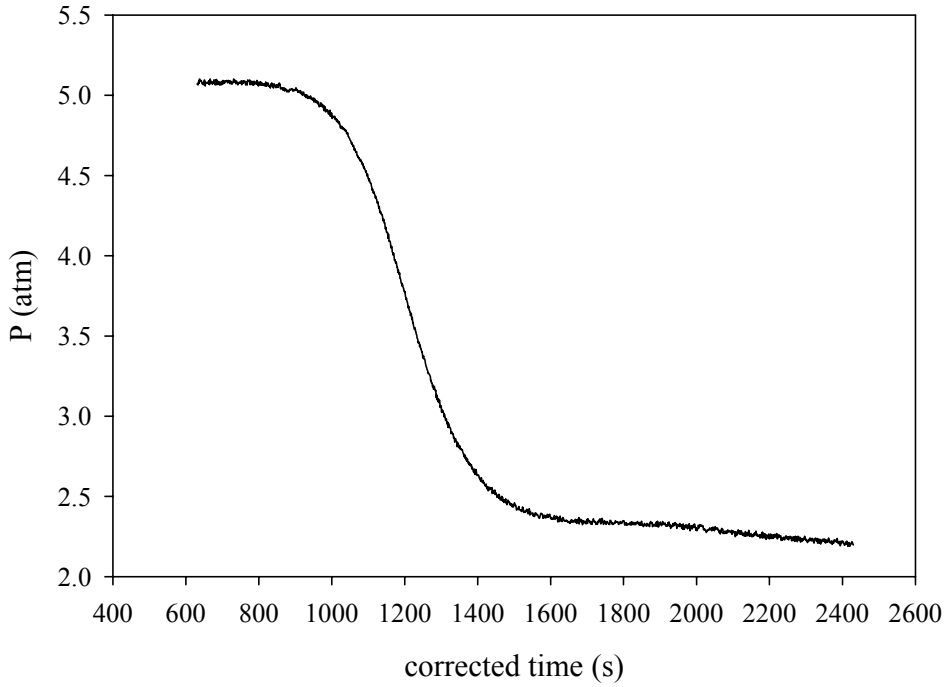

Figure 14: Composition and pressure curves for the initial hydriding of VTiNi.

The VTiNi sample was subjected to dehydriding to observe the amount of reversible hydrogen in the sample. The thermogram (Figure 15) and the percent hydrogen desorbed (Figure 16) indicate the release of hydrogen started at approximately room temperature and continued up to 350 ºC, the maximum temperature used in the experiment. At this point only about 0.4% of the absorbed hydrogen was given off. Then as the cooling started, the sample appeared to reabsorb the hydrogen that was previously released.

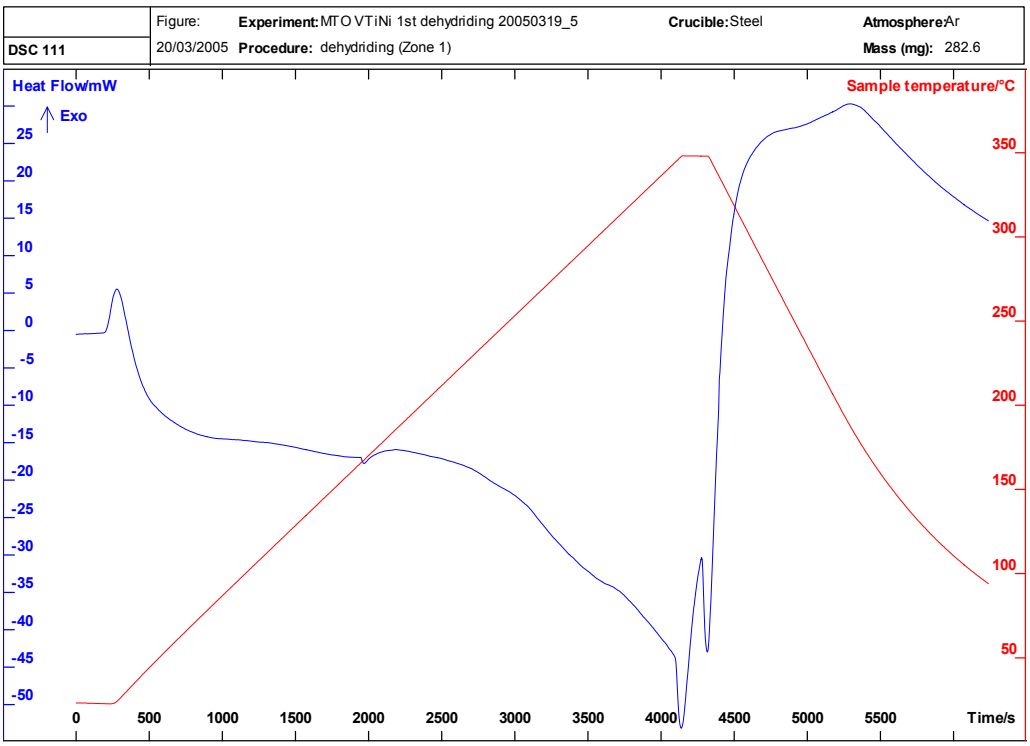

Figure 15: Thermogram for dehydriding of VTiNi.

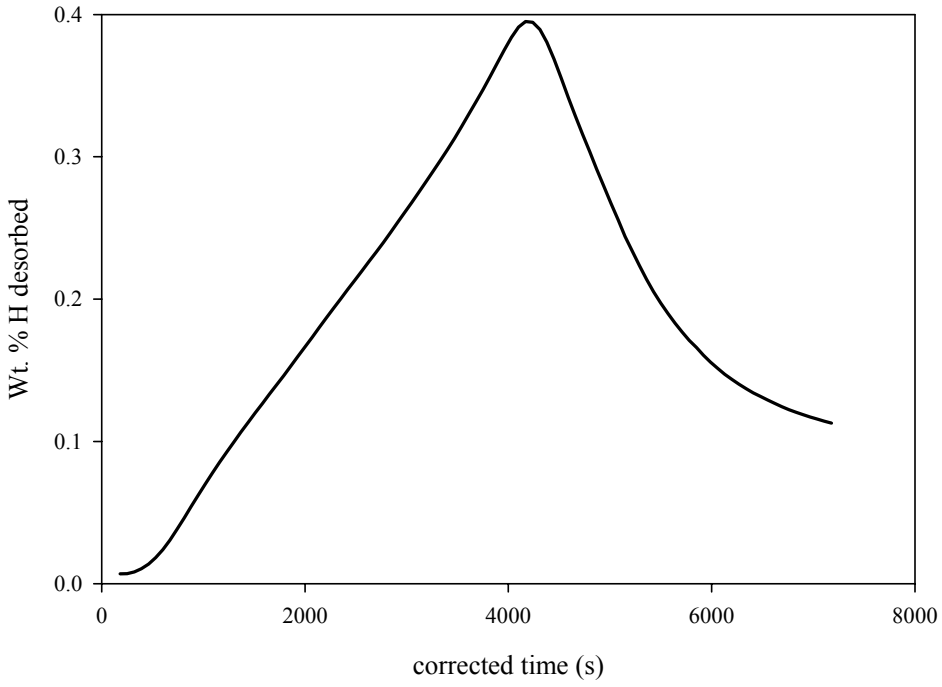

Figure 16: Percent hydrogen desorbed for dehydriding of VTiNi.

Even though the hydrogen uptake onset temperature of the VTiNi alloy was less than that of Mg_2Ni, it had a lower hydrogen capacity at about 5 atm of initial H_2 pressure. Hydriding of the sample was complete in about 15 minutes, similar to Mg_2Ni.

3.1.3. $LaNi_5$

The hydrogen uptake properties of $LaNi_5$ samples were determined under isothermal conditions at room temperature. This was possible because $LaNi_5$ forms a

solid solution of hydrogen rather than a covalent or metallic hydride as in the case of Mg_2Ni, which required a considerable energy input to initiate the reaction with hydrogen.

The $LaNi_5$ used in the first part of this study was obtained from Ergenics Inc. Unfortunately, Ergenics, Inc. stopped supplying the material and so the remainder of the work was done with alloy obtained from Alfa Aesar. The $LaNi_5$ obtained from Ergenics Inc. was shown to have a higher hydrogen capacity than the alloy obtained from Alfa Aesar but was otherwise a comparable material.

Samples were activated for hydrogen uptake by ball milling and subsequent thermal treatment in a hydrogen atmosphere. The effects of ball to powder ratio and the type of mill on the activation of the alloy were studied.

3.1.3.1. Effect of Ball Milling

Approximately 200 mg of $LaNi_5$ were directly transferred to the DSC sample boat without any treatment. The sample was subjected to thermal activation then was pressurized again with 5 atm H_2 and pressure was monitored at constant temperature. As no change in pressure, it is assumed that the sample did not react with hydrogen significantly. A second activation cycle was performed followed by the second constant temperature hydriding; however, the sample still did not react with hydrogen. In both of the constant temperature experiments, the non-milled sample took up only 0.05% H.

The next $LaNi_5$ sample was prepared by ball milling in Spex8000 Mixer Mill for 10 minutes with a ball to powder ratio (BPR) of 10:1. Approximately 200 mg of sample

were placed in the DSC. The cell was pressurized with about 4 atm H_2 and pressure was monitored at constant temperature to determine if ball milling alone activated the sample for hydrogen uptake. Pressure remained constant during the experiment, implying that the sample was not active.

3.1.3.2. Effect of Thermal Activation

The sample described above (section 3.1.3.1) was then subjected to a thermal activation cycle, followed by constant temperature hydriding at 5 atm H_2. Pressure and thermal monitoring started immediately after the system was sealed. Pressure dropped instantly along and corresponded to the exotherm shown in the thermogram in Figure 17. The sample took up 1.02% H rapidly, Figure 18.

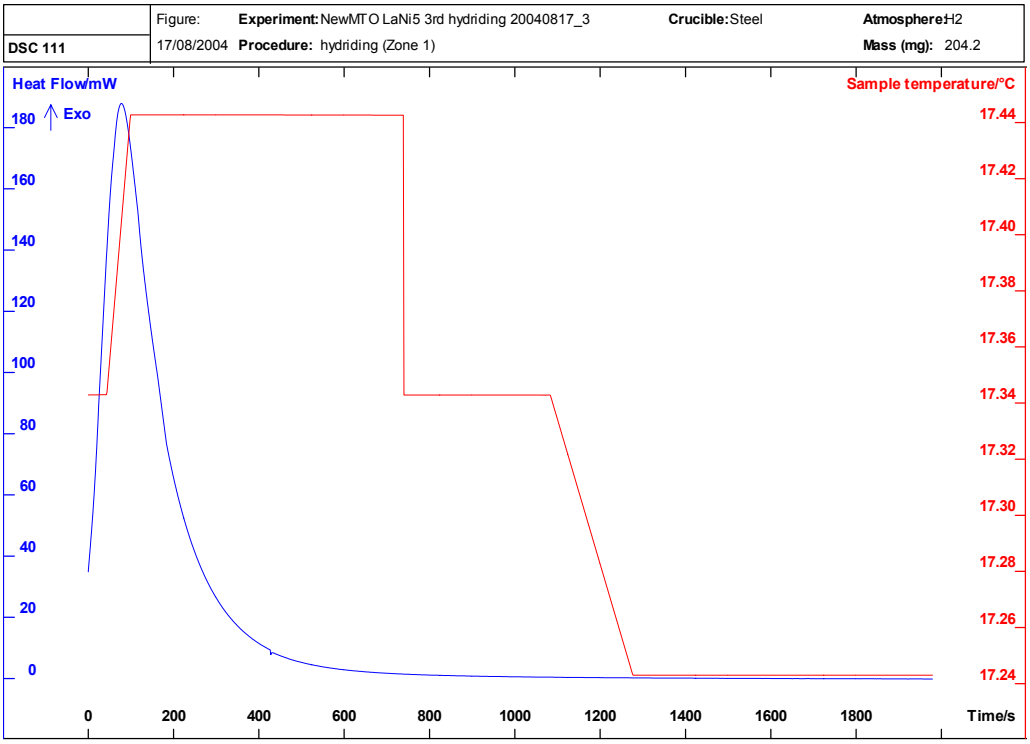

Figure 17: Thermogram of ball milled and thermally activated $LaNi_5$.

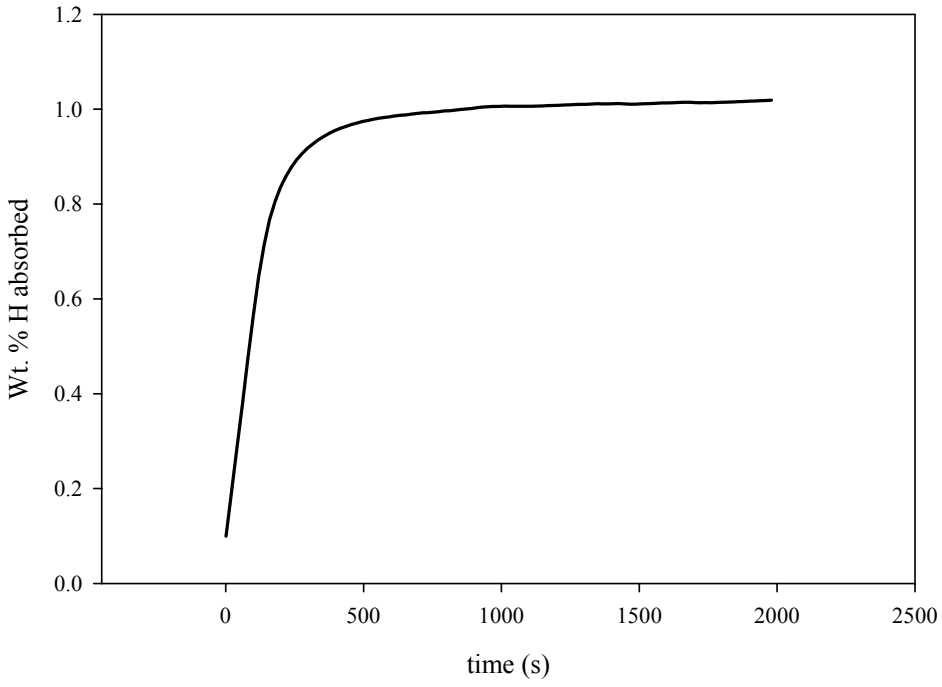

Figure 18: Composition curve of ball milled and thermally activated $LaNi_5$.

The average value of percent hydrogen for the sample described was calculated as 1.04% ($LaNi_5H_{4.5}$). Mechanical milling, followed by a single hydriding/dehydriding cycle resulted in the activation of $LaNi_5$. This was explained by the generation of new surfaces by cracking due to cell volume expansion upon hydriding [62]. The percent hydrogen obtained, as opposed to the theoretical value of 1.57% ($LaNi_5H_{6.7}$), was most likely due to the application of different activation procedures and experimental parameters, such as low H_2 pressure. It was reported previously that at high H/M ratios corresponding to the full hydride $LaNi_5H_{6.7}$, reproducibility is reported to be markedly affected by extrinsic experimental conditions and intrinsic properties, such as compositional variances, of $LaNi_5$ [53].

The results of DSC analyses were dependent on several uncontrolled experimental parameters. For instance, from the milled samples, only a portion was taken for hydrogen uptake analysis, and the analyzed portion may not have been representative of the whole. The size of the sample taken to the DSC was another variable, at low pressures the amount of H_2 was not enough to fully hydride the sample. Smaller samples had higher hydrogen capacities due to the more H_2 per unit mass of sample.

3.1.3.3. Effects of Type of Mill, Milling Speed and Milling Atmosphere

Additional $LaNi_5$ was milled using a Fritsch Pulverisette Planetary Mill. Milling was done for 10 minutes, with a ball to powder ratio of 10:1. Milling speeds of 100 rpm and 300 rpm were chosen to observe the effect of those parameters on activation. In the

100 rpm setting, the milling vial was filled with 20 balls and 8.01 grams of sample. After milling, it was observed that the sample still contained the coarse particles. After thermal activation in the DSC, the sample did not absorb hydrogen in the subsequent constant temperature hydriding. Then, the milling speed was changed to 300 rpm for the next sample. After the activation cycle, 0.60% H was absorbed by the alloy, corresponding to $LaNi_5H_{2.6}$ (Figure 19). The use of higher milling speed resulted in activation of the sample. Even though the reaction reached equilibrium within the first 500 seconds, similar to the sample prepared using the Spex8000 Mixer Mill, hydrogen capacity was lower. The reason for this difference in hydrogen capacity was possibly due to the different milling speeds which were 1725 rpm in Spex8000 and 300 rpm in the Fritsch. At higher milling speeds, the impact on the particles were stronger and the stress induced was more pronounced.

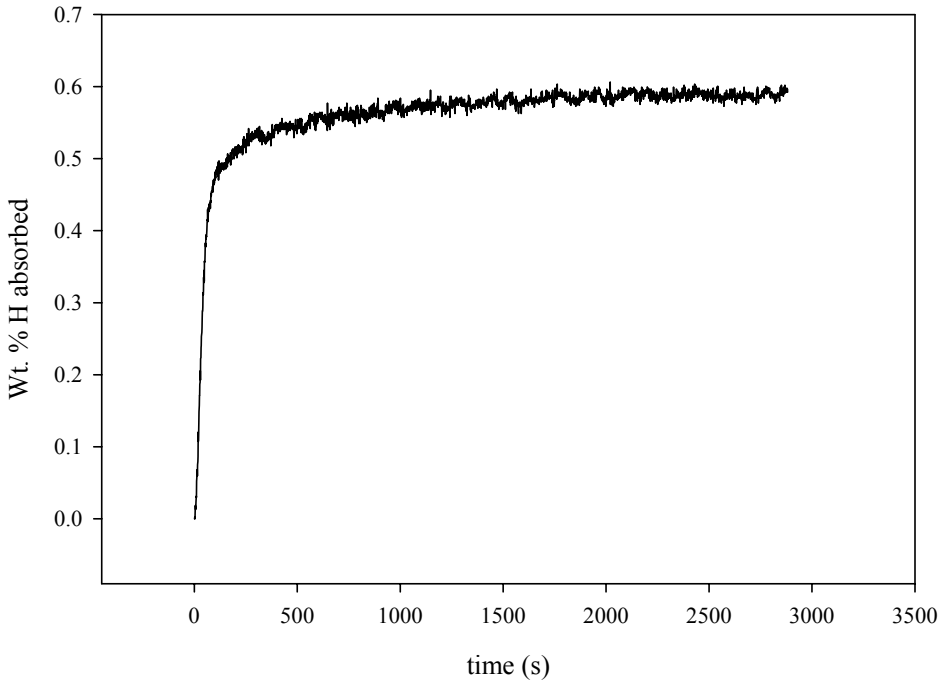

Figure 19: Composition curve for hydriding of $LaNi_5$ prepared in Fritsch Pulverisette Mill at 300 rpm.

In an attempt to enhance activation by milling, the vial containing the sample was filled with 3.7 atm H_2 prior to milling. Milling in a reactive atmosphere is referred to as reactive milling. This was accomplished by using a vial cap equipped with inlet and outlet valves to change the milling atmosphere. This type of vial was only available for the Fritsch Pulverisette mill. By reactive milling, it was projected to increase the brittleness of the alloy by the dissolution of hydrogen in the metal, inducing lattice expansion in the crystal structure and causing internal stress. The sample took up 0.56% H after thermal activation, which was less than, but close to, the value determined for the sample prepared in an argon atmosphere. It was reported previously that reactive milling under approximately 10 atm of H_2, using similar milling parameters (Fritsch mill, 30:1

BPR, 400 rpm, 5 minutes) did not result in any improvement in terminal hydrogen capacity [63]. As milling time was increased (60 to 600 minutes), H_2 capacity decreased for samples that were milled under both Ar and H_2 atmospheres. Samples milled in hydrogen showed a greater decrease in hydrogen capacity due to formation of elemental La and, consequently, its thermodynamically stable hydride LaH_2. On the other hand, the kinetics for both systems were enhanced as the plateau region in the p-c-T diagram diminished (Figure 20) indicating the disappearance of the $LaNi_5$ hydride phase [63].

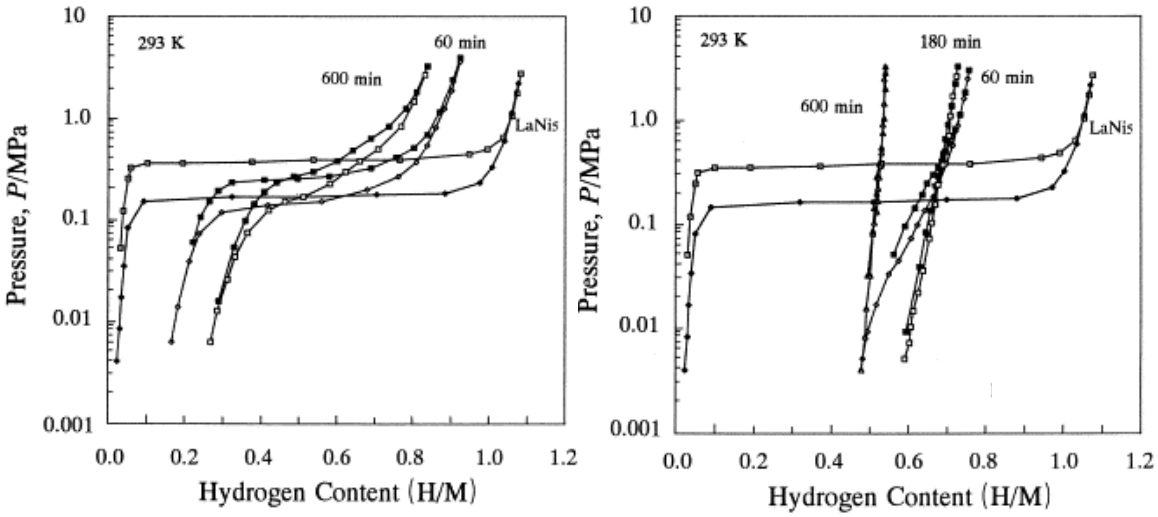

Figure 20. Effect of milling time on pressure-composition isotherms of $LaNi_5$ under argon (left) and hydrogen (right) atmospheres.

3.1.3.4. Effect of Milling Time and Ball to Powder Ratio

Two samples of $LaNi_5$ were milled in the Spex8000 Mixer Mill with a BPR of 1:1 for 10 and 30 minutes, respectively. Each sample was analyzed for hydriding at constant temperature after a single activation cycle. The% H absorbed by the samples, along with the results presented in the previous sections, are given in Table 1. The data indicate that $LaNi_5$ was best activated with the Spex8000 Mixer Mill with a BPR of 10:1 for 10 minutes.

During ball milling, some of the material was stuck on the milling media. In the Spex8000M mill with 10:1 ball to powder ratio, the amount of $LaNi_5$ lost was 30% of the initial amount. To avoid material loss, samples for larger scale experimentation were prepared with a lower BPR. BPR and milling time were 1.7:1 and 30 minutes, respectively. Those samples were also analyzed using the DSC. The DSC analyses included the activation cycle, followed by the constant temperature hydriding and were repeated five times. The average percent hydrogen capacity at about 5 atm of H_2 was calculated to be 0.76%.

Table 1: Effects of various milling parameters on hydrogen capacity.

	Mill type						
Milling variables	Fritsch Pulverisette			Spex8000			
Milling vial	SS[a]	SS	SS	WC[b]	WC	WC	SS
Atmosphere	Ar	Ar	H_2	Ar	Ar	Ar	Ar
Speed, rpm	100	300	300	1725	1725	1725	1725
BPR	10:1	10:1	10:1	10:1	1:1	1:1	1.7:1
Milling time, min	10	10	10	10	10	30	30
% H	None	0.60	0.56	1.06	0.54	0.66	0.76

[a] Stainless steel
[b] Tungsten carbide

3.1.3.5. Dehydriding of $LaNi_5$

The thermogram representing the dehydriding of $LaNi_5$ is shown in Figure 21. Of the two endotherms; one was observed during the delay of heat transfer to the sample, and the other after heating started. This indicated that some hydrogen was released at room temperature (Figure 22), and then after heating starts the rest was given off. Dehydriding was complete when the sample temperature reaches about 340 K.

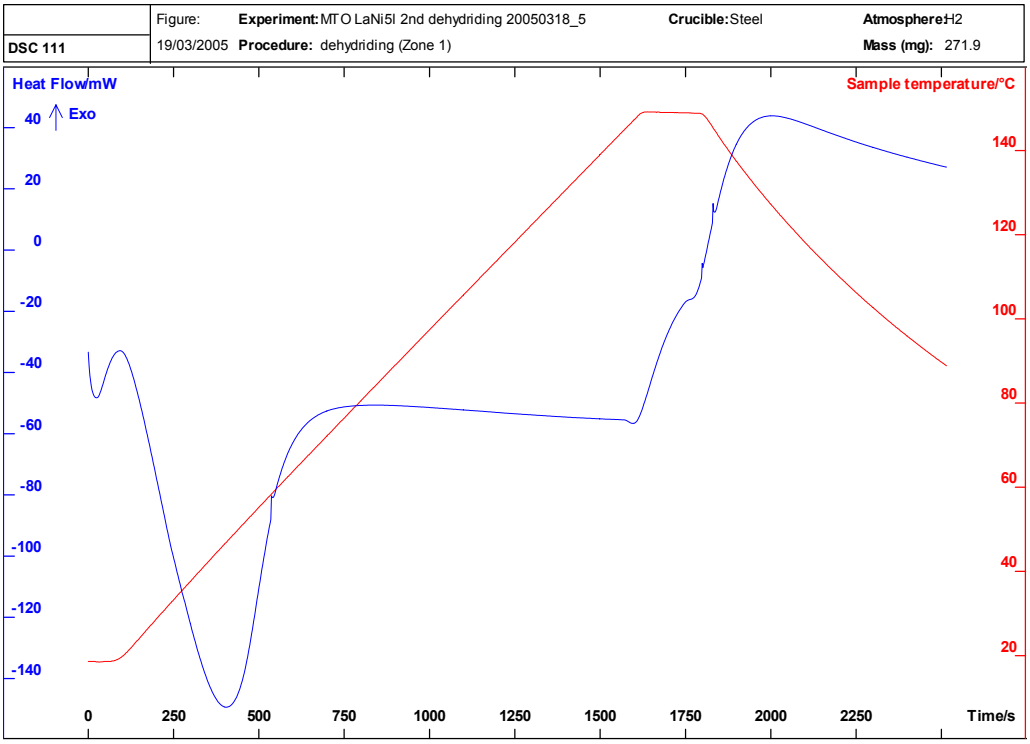

Figure 21: Thermogram for dehydriding of $LaNi_5$ starting with 1 atm. H_2.

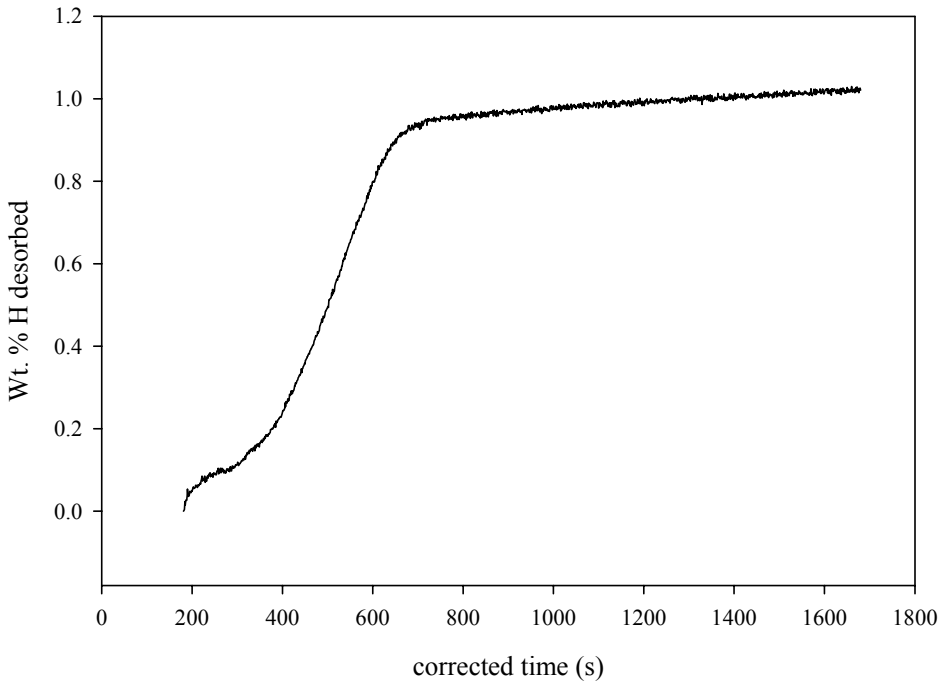

Figure 22: Percent hydrogen desorbed plot for dehydriding of $LaNi_5$.

Due to the fast kinetics observed at ambient temperatures, $LaNi_5$ was subjected to further analysis as a candidate material for hydrogen recovery from H_2:He mixtures. The effects of the addition of aluminum by ball milling, as well as varying the preparation parameters, have been investigated and the results are presented in the following sections.

3.2. Aluminum in $LaNi_5$

3.2.1. Interaction With Pure Hydrogen

The effect of partial substitution of nickel by aluminum in $LaNi_5$ for the purpose of altering the hydriding properties has been subject of many previous studies. From the macro perspective, lower H_2 pressure was needed to achieve the same H/M ratio as $LaNi_5$ alone. This observation is explained from the effect of Al on the crystal lattice expansion upon hydriding, which is a limiting factor to the process. Aluminum addition is reported to decrease the extent of expansion by decreasing the dislocation density and vacancy concentration upon hydriding. It also increases the lattice constants, resulting in more hydrogen being absorbed [58].

In the previous studies, $LaNi_{5-x}Al_x$ samples were reported to be prepared by arc melting the stoichiometric amounts of the components followed by size reduction by ball milling. In this study, aluminum was added to $LaNi_5$ via ball milling. Therefore, the Al content is presented as mole percentages, varying between approximately 0.9 and 33.3 % of the total number of atoms in $LaNi_5Al_x$.

In this section, results of the DSC analyses are presented. The results of the scaled up analyses which were done using the Parr reactor and the U-tube reactor are given in the subsequent sections. Experimentally determined aluminum content for all the samples are presented in this section.

The theoretical mole percentages of Al in $LaNi_5Al_x$ in DSC analyses were 0.87, 5.26, 14.29 and 33.33 mole %. Percentages for samples used in Parr and U-tube reactors were 0.79, 1.56, 3.88 and 14.21 mole %. The actual percent Al values were determined after the samples had been ball milled and used for hydrogen uptake. Some of the samples were analyzed before they were reacted with hydrogen. The results for all samples, converted to mole % Al, are given in Table 2.

Table 2. Aluminum content before and after ball milling.

		Mole % Al	
	Sample	Initial mixture	After Milling
1.	Milled (SS), reacted, *Parr*	*0.79*	*0.74*
2.	Milled (WC), reacted, *DSC*	*0.87*	*0.77*
3.	Milled (SS), reacted, *Parr*	*1.56*	*1.35*
4.	Milled (SS), *Parr*	*1.56*	*1.22*
5.	Milled (SS), loose powder, *Parr*	*3.88*	*3.38*
6.	Milled (SS), residue in the vial, *Parr*	*3.88*	*3.94*
7.	Milled (WC), reacted, *DSC*	*5.26*	*4.74*
8.	Milled (SS), *Parr*	*14.21*	*14.00*
9.	Milled (WC), reacted, *DSC*	*14.29*	*12.00*
10.	Milled (WC), reacted, *DSC*	*33.33*	*47.31*

The mole % Al after milling was less than that was originally loaded except for samples 6 and 10. Sample 6 was the material that was stuck on the milling media. The stuck material was recovered by milling the remaining powder in the presence of ethanol and then filtering the metal-ethanol suspension and drying. Al was the more malleable component, therefore, during milling it coated the milling media and depleted in the bulk. The increase of Al content in sample 10 may be because of the non-homogeneity of the milled product, therefore, the sample taken for analysis may not have been representative of the whole.

Weight percent of H absorbed by $LaNi_5$+Al samples are listed in Table 3 and the H_2 uptake curves for the samples containing different amounts of Al are given in Figure 23. The closeness of percent hydrogen for smaller percent Al was due to the poor reproducibility of this heterogeneous reaction.

Table 3: Percent hydrogen uptake values for different amounts of Al in $LaNi_5$.

	Mole % Al				
Wt. % H	0	0.77	4.74	12.00	47.31
Avg. (n=3)	1.04	1.05	0.95	0.87	0.68
Max. observed	1.09	1.13	0.98	0.92	0.69

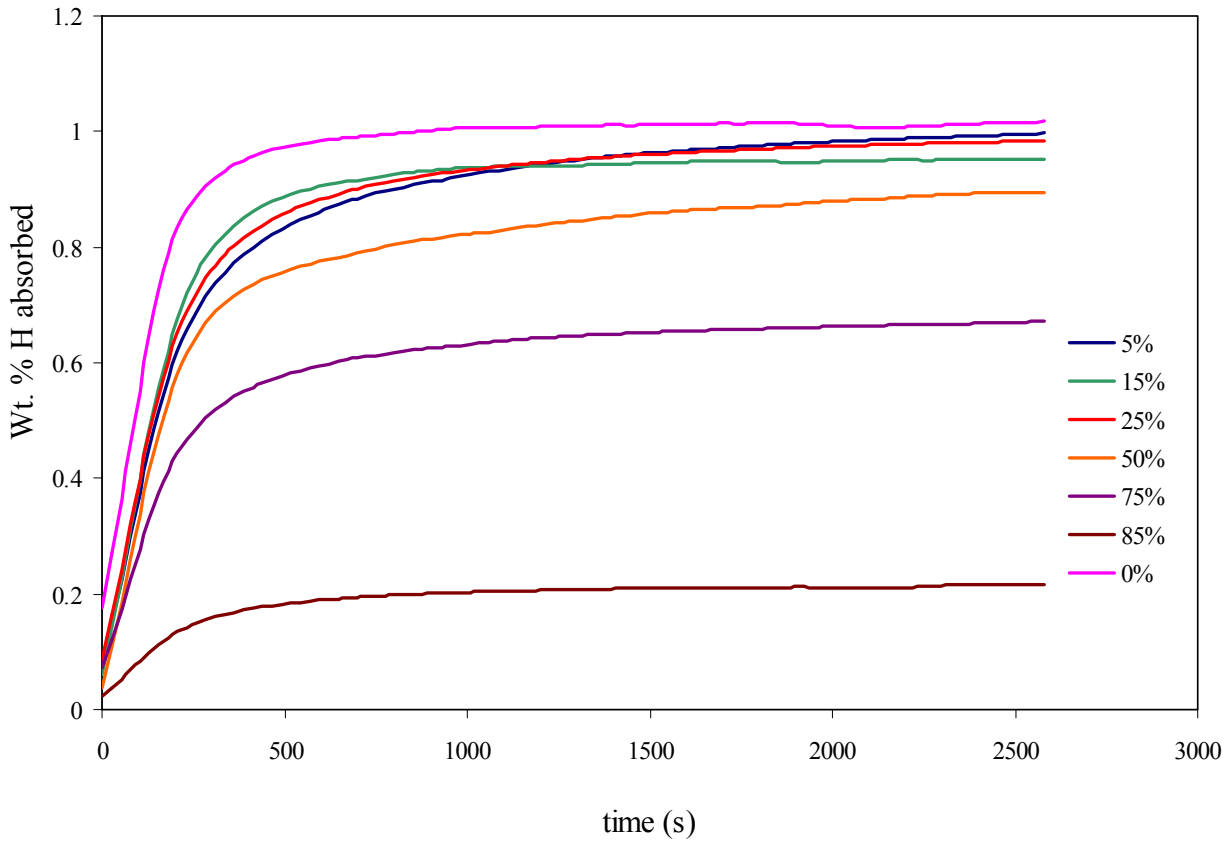

Figure 23: Percent hydrogen uptake curves for different amounts of Al in $LaNi_5$

Dependence of percent hydrogen absorbed on Al content in $LaNi_5$ is given in Figure 24. The observed amount of H_2 absorbed remained constant at low Al contents, and then decreases as Al content increased.

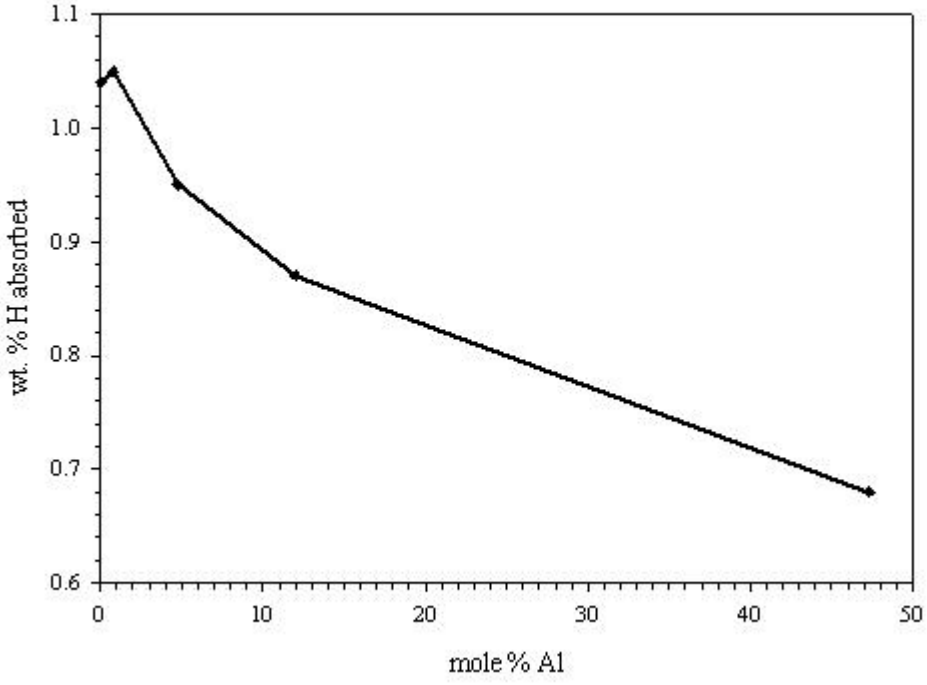

Figure 24: Percent hydrogen capacity as a function of mole % Al in $LaNi_5$.

3.2.2. Hydrogen Uptake From Hydrogen – Helium Mixtures

VTiNi, $LaNi_5$ and $LaNi_5$ with 0.77, 4.74 and 12.00 mole % Al were subjected to hydriding tests using a mixture of 50% (v/v) hydrogen and helium. Mg_2Ni was excluded from analyses with H_2:He mixtures due to its high hydriding onset temperature.

3.2.2.1. VTiNi

VTiNi was first hydrided with H_2 only. Then VTiNi was analyzed with He at 150 ºC at 40 psig pressure as the control reaction. The pressure data proves (Figure 25) VTiNi does not interact with pure He.

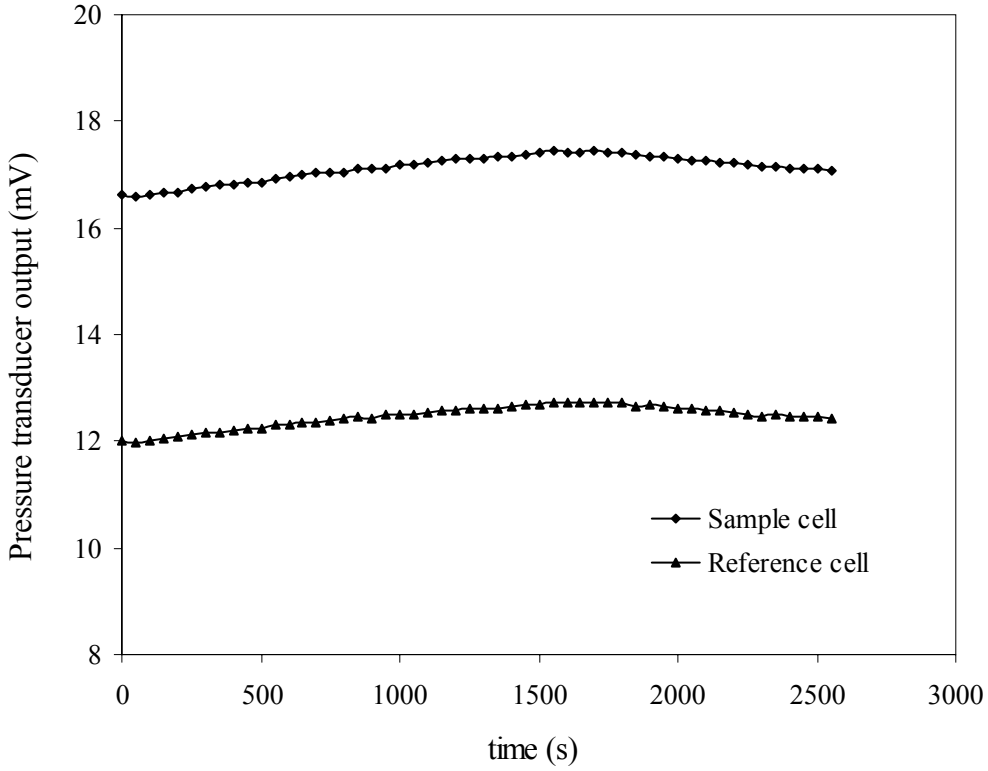

Figure 25: Pressure transducer output curve for VTiNi heated under He atmosphere.

Then, the DSC cells were filled with a 50% H_2:He (v/v) mixture and the sample was subjected to hydriding with heating up to 150 ºC. The associated thermogram (Figure 26) shows two exotherms. The first is due to an undetermined experimental parameter at

the start of the heating period, which is observed in every other experiment. The second exotherm starting at approximately the 800th second is accompanied by a pressure drop. The percent hydrogen versus corrected time plot given in Figure 27 (b) and that of hydriding with pure H_2 (a) indicates approximately 0.2 % H is absorbed. In the presence of helium, hydriding occurs in one step similar to the case of pure hydrogen however, both the rate of uptake and terminal capacity of hydrogen in VTiNi are reduced.

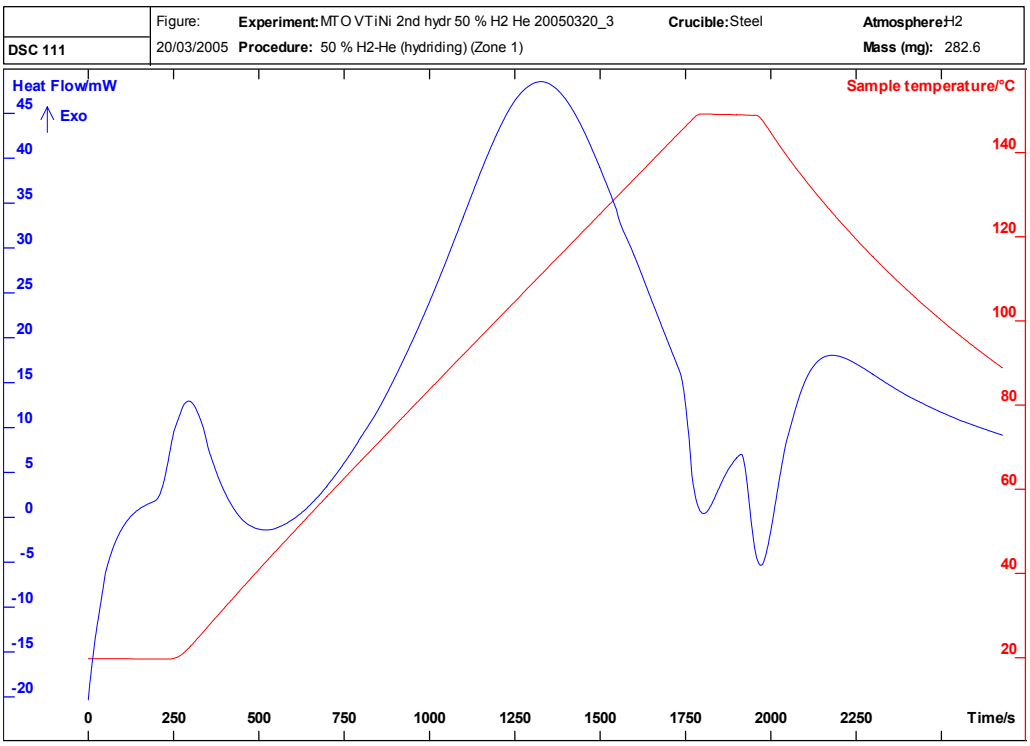

Figure 26: Thermogram of VTiNi hydrided with 50% (v/v) H_2-He mixture.

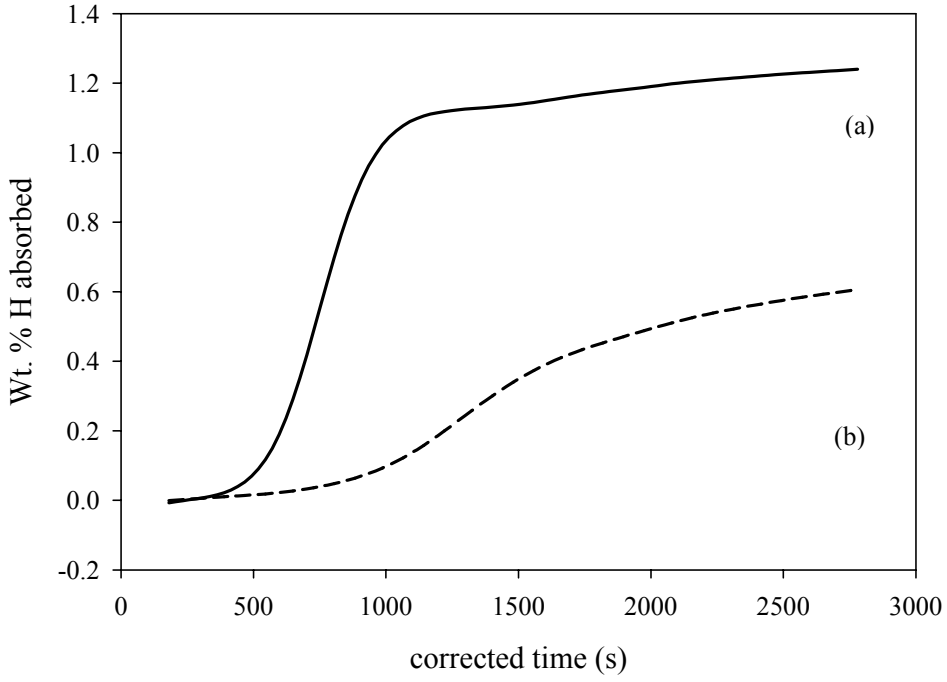

(a) Under H_2, partial pressure of H_2 = 5.07 atm.
(b) Under 50% H_2-He (v/v), partial pressure of H_2 = 3.31 atm.

Figure 27: Percent hydrogen curves of VTiNi hydrided with 50% (v/v) H_2-He mixture and pure H_2.

3.2.2.2. $\underline{LaNi_5}$

The percent hydrogen release profile with time is given in Figure 28, including that of $LaNi_5$ hydrided with pure H_2. After initial uptake of hydrogen of about 0.08%, about 0.38% terminal hydrogen capacity was reached in the following several hours. The presence of helium was shown to slow down the reaction and reduce hydrogen capacity.

However, it was noted that the partial pressures of H_2 in the two cases were different, which will be addressed in the following sections where H_2 pressure is constant.

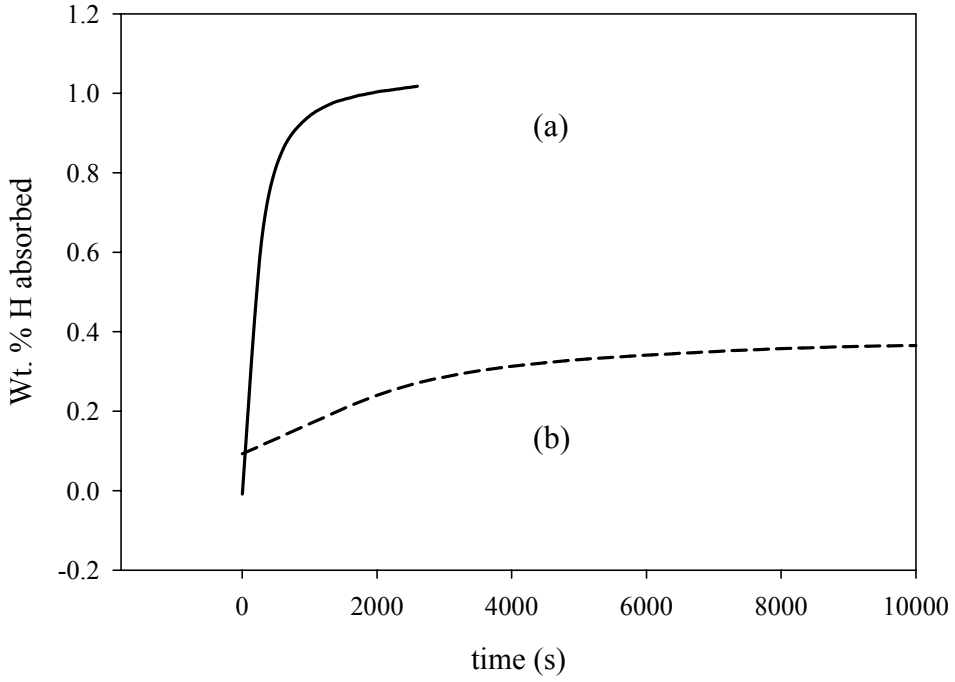

(a) Under H_2, partial pressure of H_2 = 5.11 atm.
(b) Under 50% (v/v) H_2-He, partial pressure of H_2 = 3.33 atm.

Figure 28: Percent hydrogen curves of $LaNi_5$ hydrided with 50% (v/v) H_2-He mixture and pure H_2.

3.2.2.3. $LaNi_5$ with Al

The sample containing 12% Al was pressurized with pure He to verify inertness. There was no pressure drop observed (Figure 29); therefore, all samples of $LaNi_5$ and $LaNi_5Al_x$ were accepted to be non-interacting with He.

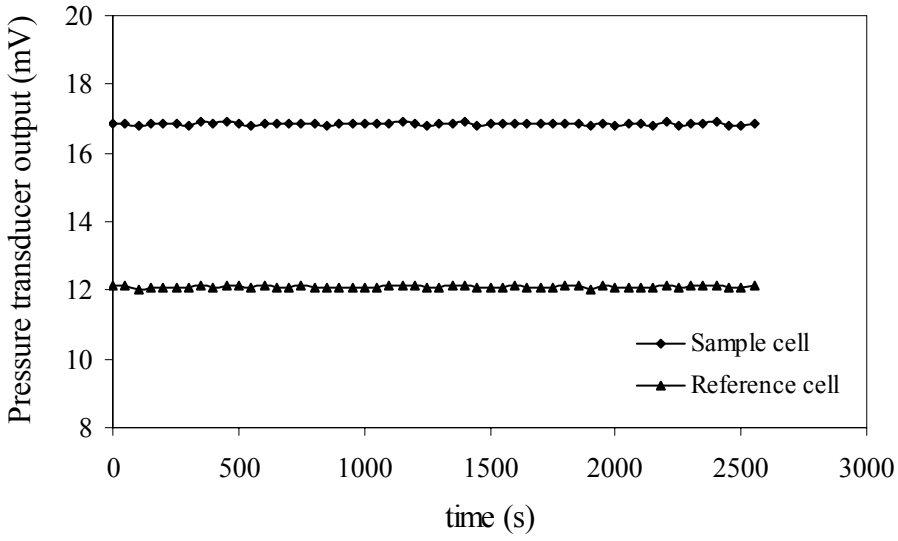

Figure 29: Pressure transducer output of DSC for 50 mole % Al in $LaNi_5$ under pure He atmosphere.

$LaNi_5$ samples containing 0.77, 4.74 and 12.00 mole % Al were hydrided using 50% (v/v) H_2-He mixture, as described for pure $LaNi_5$ in section 3.2.2.2, using two different pressures, 6.6 and 10 atm. The amounts of hydrogen absorbed at different H_2 partial pressures are given in Table 4. For all the samples, percent hydrogen absorbed was similar, provided that the partial pressures of H_2 were equal. For lower partial pressures,

percent hydrogen was decreased. The amount of H absorbed was found to be dependent on the initial pressure of H_2.

Table 4. Dependence of percent hydrogen absorbed on partial pressure of H_2.

	Atmosphere	P_{H2}, atm.	Wt. % H
$LaNi_5$	H_2	*5.11*	*1.02*
	50% (v/v) H_2-He	*3.33*	*0.36*
0.77 mol % Al in $LaNi_5$	H_2	*5.60*	*1.05*
	50% (v/v) H_2-He	*3.30*	*0.33*
	50% (v/v) H_2-He	*5.10*	*0.90*
4.74 mol % Al in $LaNi_5$	H_2	*5.07*	*0.97*
	50% (v/v) H_2-He	*3.35*	*0.35*
	50% H_2-He	-	-
12.00 mol % Al in $LaNi_5$	H_2	*5.27*	*0.80*
	50% (v/v) H_2-He	*3.37*	*0.15*
	50%(v/v) H_2-He	*5.10*	*0.59*

The percent hydrogen curve for the sample with 0.77% Al (Figure 30) at 5 atm of H_2 indicated a decreased reaction rate with the presence of helium. The completion time for the reaction dropped from about 10 minutes to 120 minutes.

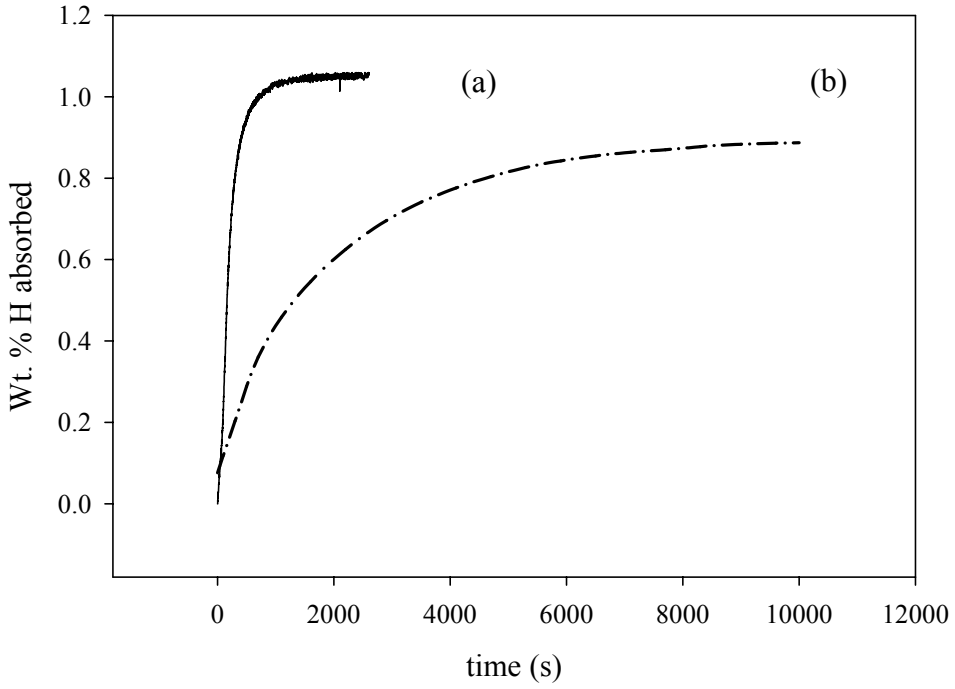

Figure 30: Percent hydrogen curves for $LaNi_5$ with 0.77% Al, hydriding under pure H_2 (a) and 50% (v/v) H_2-He (b).

The decreased reaction rate of hydrogen uptake of $LaNi_5$ due to the presence of helium was previously reported and the rate limiting step was announced to be the transport of H_2 to the surface of the $LaNi_5$ [64]. This result was verified in this work. Supported with the inertness of $LaNi_5$ with He, the rate limiting step was verified to be the transport of H_2 from the bulk of the gas phase to the metal gas interface.

3.2.2.4. AuPd and Pt Coating on $LaNi_5$

The reduced reaction rate for the H_2-$LaNi_5$ system was determined to be the inhibition of transport of H_2 to the $LaNi_5$ surface. The dominance of He on the surface eventually left less surface for H_2 absorption. On the other hand, the capacity was not highly affected due to the fact that interaction of the metal with H_2 was inhibited only at the surface.

Gold-palladium (AuPd) and Platinum (Pt) are known to be used as catalysts facilitating hydrogen dissociation in hydrogenation reactions. The dissociation and transport of H_2 is expected to be high on these catalysts. Therefore to overcome the inhibition of rate when He is present (i.e. enhance H_2 dissociation on the surface), the samples were coated with AuPd and Pt.

The percent hydrogen values for $LaNi_5$ with 12 and 0.77% Al at different hydriding pressures are given in Table 5. The types of coating and percent hydrogen values for non-coated samples as reference are also listed.

The amount of hydrogen absorbed from 50% (v/v) H_2-He mixtures increased as AuPd coating times increased. The percent hydrogen was still less than the value obtained from pure H_2 at the same pressure. However, the capacity loss in the presence of He was restored for Pt coated samples.

Table 5. Percent hydrogen uptake with AuPd and Pt coating on $LaNi_5$.

Mole % Al	Coating type and time, min	Weight % H		
		5 atm H_2	5 atm H_2 in 50% (v/v) H_2-He	3.3 atm H_2 in 50% (v/v) H_2-He
12	No coating	0.81	0.59	-
12	AuPd, 4	0.91	0.64	0.33
12	AuPd, 8	0.84	0.79	0.43
12	Pt, 2	0.83	-	0.33
0.77	No coating	1.03	0.83	-
0.77	Pt, 2	1.00	1.01	0.55

Figure 31 shows percent hydrogen curves for samples with AuPd coating on 12.00% Al where the coating is shown to fail to increase the hydrogen absorption rate and capacity.

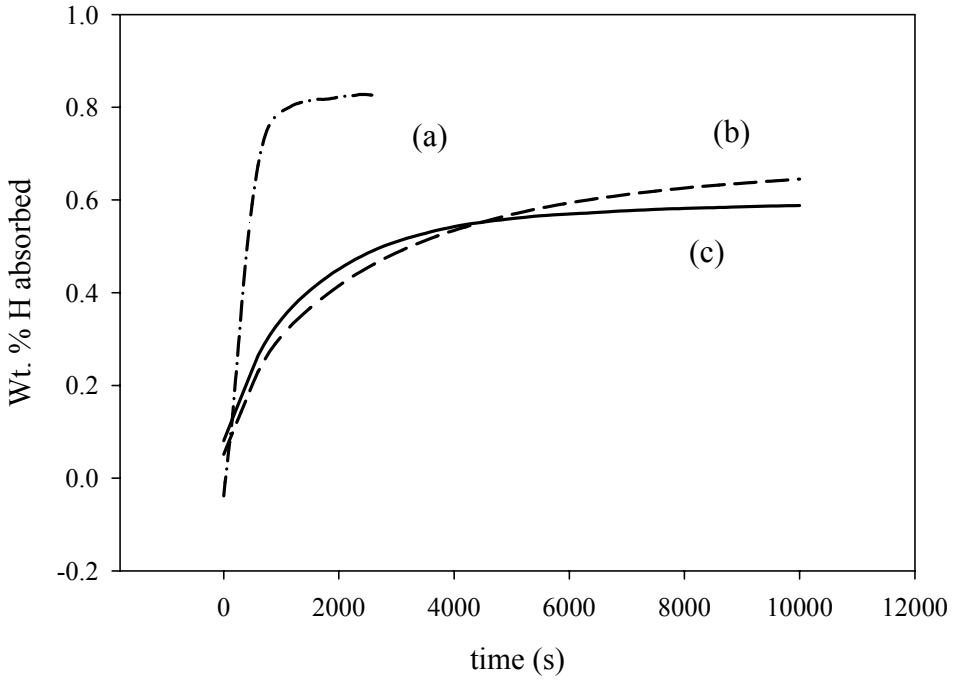

(a) non-coated, under H_2
(b) AuPd coated, under 50% (v/v) H_2-He
(c) non-coated, under 50% (v/v) H_2-He

Figure 31. Percent hydrogen curves for rate comparison of AuPd coated and non-coated samples.

The effect of Pt coating on the rate of reaction is presented in the percent hydrogen plots given in Figure 32. The time to completion of the reaction of the Pt coated sample with H_2 was about 1 hour which was lower than the 3 hour reaction time for the non-coated sample. Pt coating increased the reaction rate and capacity of $LaNi_5$ samples, which suggested the surface affinity of H_2 was enhanced. This could be due to the high solubility of H_2 in Pt.

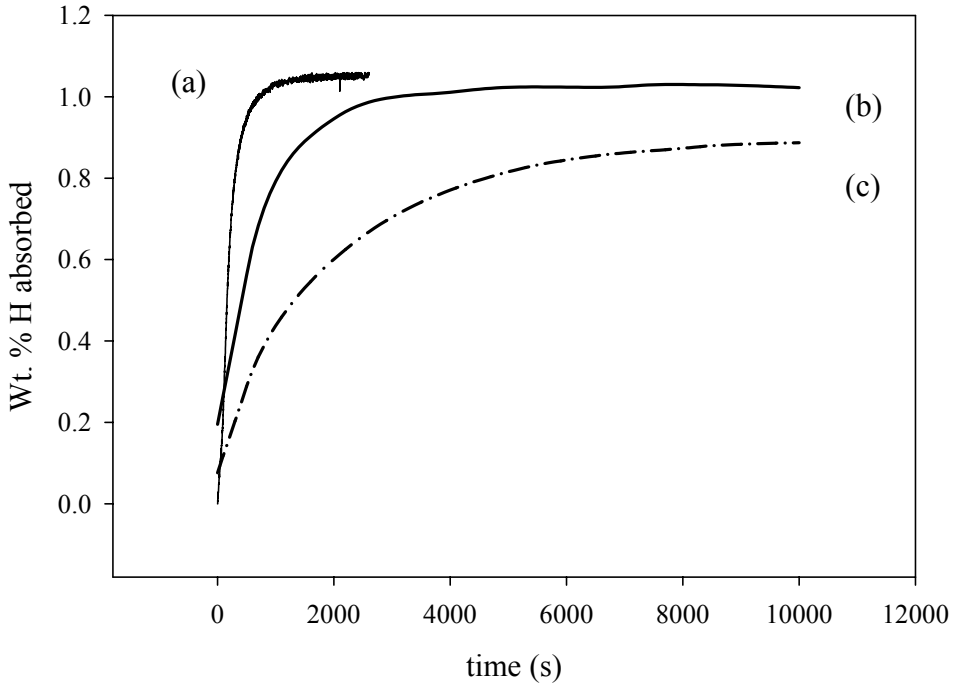

(a) non-coated, under H_2
(b) Pt coated, under 50% (v/v) H_2-He
(c) non-coated, under 50% (v/v) H_2-He

Figure 32. Percent hydrogen curves for rate comparison of Pt coated and non-coated samples.

3.3. Parr Reactor

Samples of $LaNi_5$ with 0.74, 1.35 and 3.38% Al were tested in the Parr reactor. After the activation procedure, the reactor was pressurized with H_2 sealed. Pressure drop was monitored and the percent hydrogen absorbed was calculated using the ideal gas law.

After dehydriding by the sample, the same procedure was repeated by using 50% (v/v) H_2:He.

For the reaction of the samples with H_2, the pressure profiles were plotted (Figure 33). The reactions were complete within 10 minutes; much like the reaction of $LaNi_5$ with H_2 analyzed using the DSC. The hydrogen capacities of the samples given in Table 6 indicate the percent hydrogen absorbed by the $LaNi_5$ was also in accordance with the results obtained from DSC analysis, which were given in Table 1.

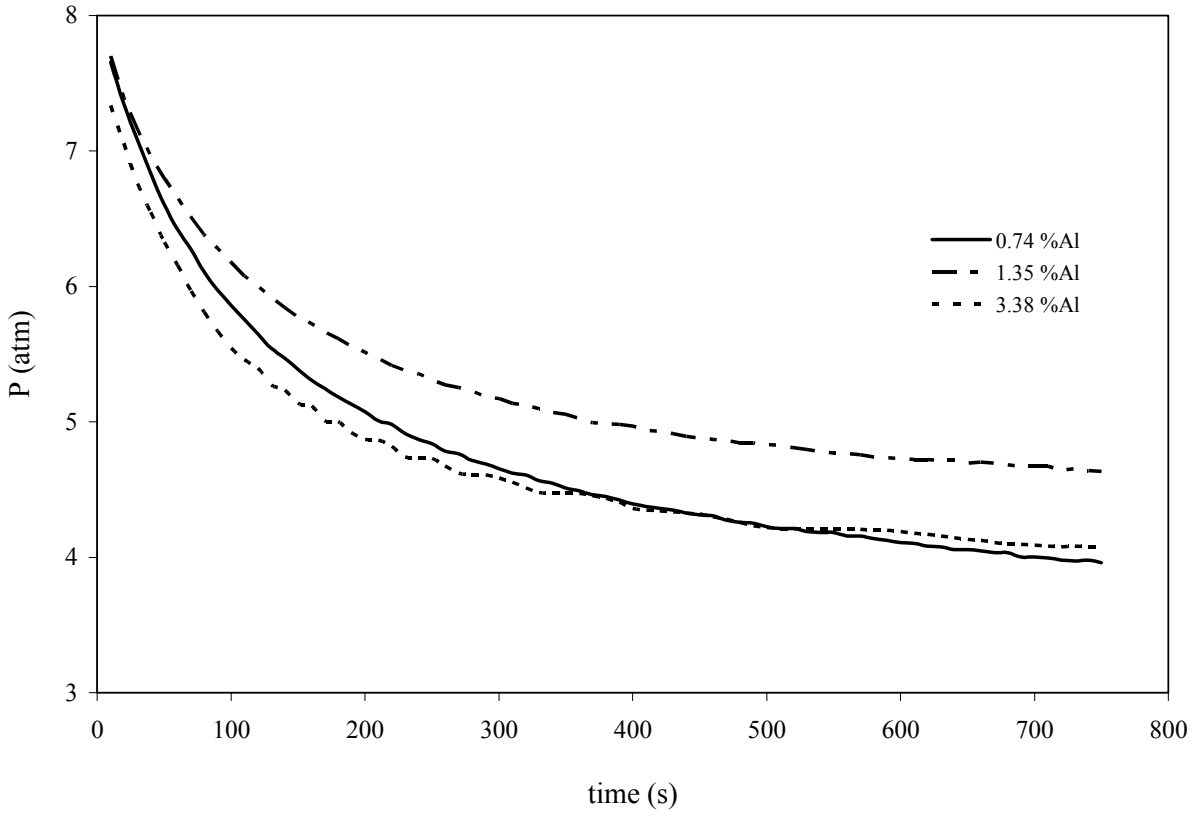

Figure 33. Pressure profiles under H_2 atmosphere.

Table 6. Percent hydrogen values for pure H_2 in the Parr reactor.

Mole % Al	P_{H2}, atm.	Weight % H
0.74	7.65	0.89
1.35	7.70	0.72
3.38	7.34	0.72

The pressure profiles for the samples that were pressurized with 50% (v/v) H_2:He (Figure 34) indicated that the reactions were complete also in 10 minutes. The percent hydrogen values are presented in Table 7. In the batch reactor, the rate of reaction was not affected from the presence of He. This observation suggests that, at high enough H_2 pressures (7 atm in 50:50 H_2:He mixture), the surface occupation of $LaNi_5Al_x$ by He was not significant, compared to low H_2 pressures (5 atm). It could also be possible that the interaction of the $LaNi_5Al_x$ with hydrogen in the presence of helium was dependent on the scale of the system. The volume of the Parr reactor was 2000 mL, as opposed to the 15.37 mL of volume of the DSC cell. Also, in the Parr reactor, the sample amount was higher. Only the top layer was exposed to the He; therefore, the surface interaction of He was limited, and a reduction in reaction rate was not observed.

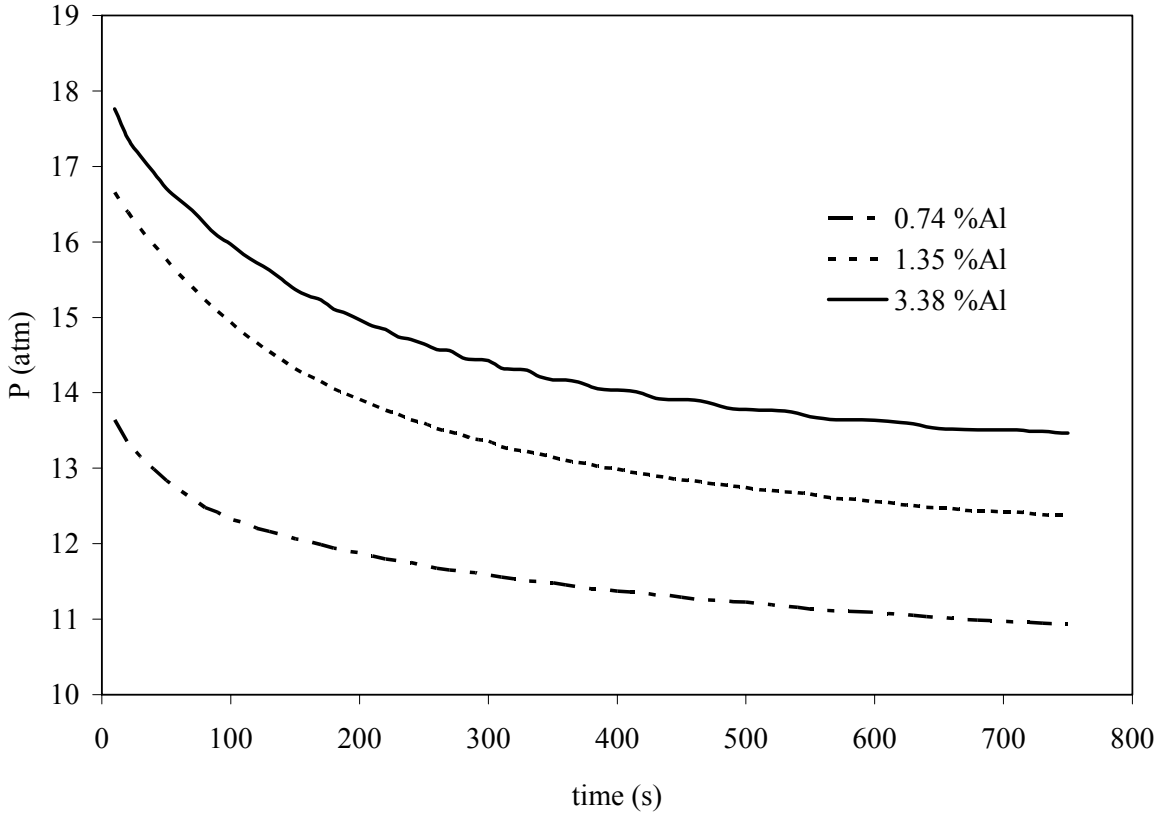

Figure 34. Pressure profiles under 50% (v/v) H_2:He atmosphere.

Table 7. Percent hydrogen values for 50% (v/v) H_2:He in the Parr reactor.

Mole % Al	P_{H2}, atm.	Weight % H
0.74	6.82	0.84
1.35	8.33	1.11
3.38	8.88	1.04

Hydrogen capacity was higher in all samples when they were hydrided using the 50% (v/v) H_2:He. Since the samples were analyzed using H_2 first, the increased percent hydrogen may indicate the samples were further activated by the first hydriding/dehydriding cycle.

3.4. U-Tube Hydriding Reactor

The U-tube that was used for scaled up experiments was filled with approximately 190 grams of $LaNi_5$ and then the flow of 2% (v/v) H_2:He at about 9 atm was fed into it. The flow out of the reactor was restricted to about 200 $mL.min^{-1}$ by a pressure relief valve. The valve maintained the pressure within the reactor, while allowing a slow flow. The gas chromatogram of multiple injections is given in Figure 35. The single peaks over the first 20 minutes were helium peaks, represented by empty circles. Hydrogen was not observed in the effluent because it reacted with $LaNi_5$. When $LaNi_5$ could not absorb any more H_2, hydrogen peaks started to show (filled circles). The percent hydrogen values in the effluent were calculated using peak area ratios of H_2 and He. The breakthrough curve was plotted as a function of time (Figure 36).

The U-tube reactor successfully removed the hydrogen from the H_2-He stream and allowed the passage of He only. The amount of hydrogen retained in the reactor at the time of saturation was calculated from material balance. The amount of helium leaving the system was calculated using flowrate and time

$$V_{He}\,(mL) = \text{flowrate}\ (mL.min^{-1}) \times \text{time}\ (min)$$

which was equal to the amount of He that entered the system. Since the composition of the entering gas mixture was known, the amount of H_2 entered was calculated using

$$V_{Hydrogen} = V_{He} \times (20/80)$$

and converted to the amount and then weight percent hydrogen in the $LaNi_5$.

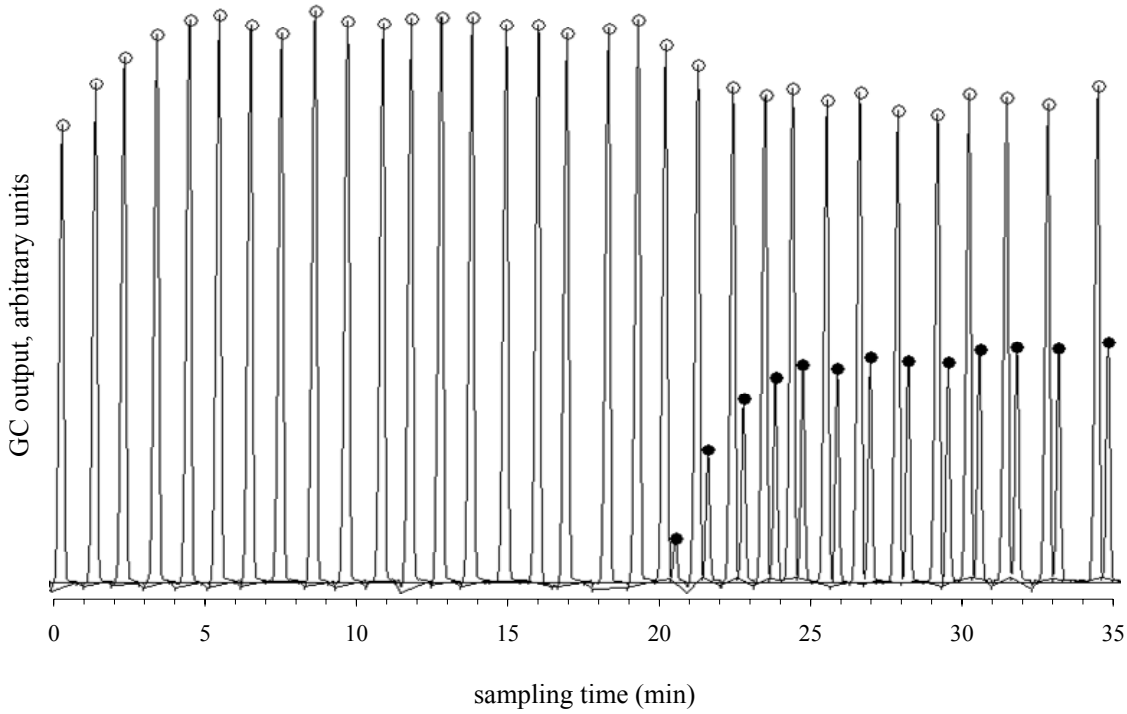

Figure 35. Chromatogram for hydrogen absorption in the U-tube reactor.

For this particular example, the percent hydrogen in the $LaNi_5$ was calculated as 0.043%. The average percent hydrogen absorbed of four trials with the same feed pressure was calculated as 0.041%. The low percent hydrogen of $LaNi_5$ was possibly due to the low pressure of H_2. The H/M ratio was 0.03, which corresponded to the α-phase as shown in the *p-c*-T diagram of $LaNi_5$ given in Chapter 1. This may indicate that the H_2 was absorbed to some extent, and the hydrogen atom concentration did not increase enough to yield the β-phase. To increase the rate of hydrogen absorption in the continuous system, and subsequently establish conditions for the formation of the hydride $LaNi_5H_6$, the partial pressure of H_2 was found necessary to be increased.

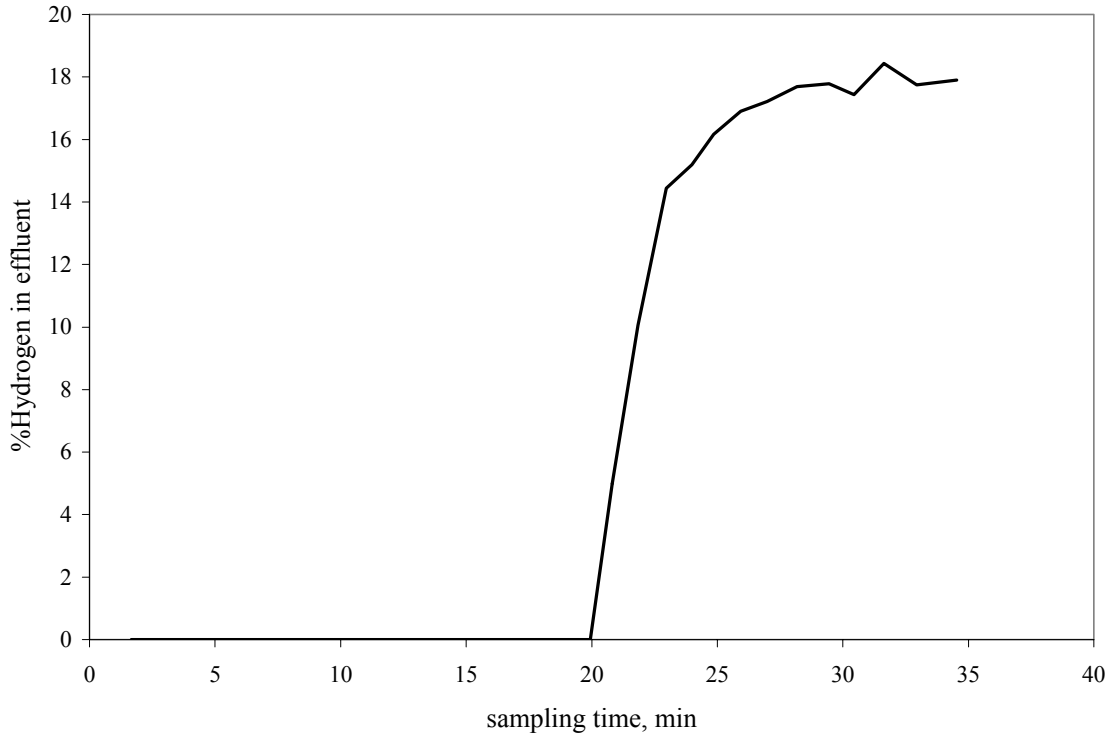

Figure 36. Effluent gas composition as percent hydrogen (v/v).

3.5. X-Ray Diffraction

3.5.1. $LaNi_5$

The $LaNi_5$ obtained from Alfa Aesar was directly transferred to the sample holder of the X-ray diffractometer without any treatment. A sample of $LaNi_5$ was loaded in the XRD and four consecutive X-ray spectra of the same sample were obtained, and given in Figure 37 along with the expected spectrum for $LaNi_5$. Inconsistencies within the peak intensities were observed, yet the elemental analysis proved that the composition of the

sample was $LaNi_5$. This may indicate that the $LaNi_5$ was not in its normal crystalline form and the energy from the X-ray beam was inducing changes in the crystal phase.

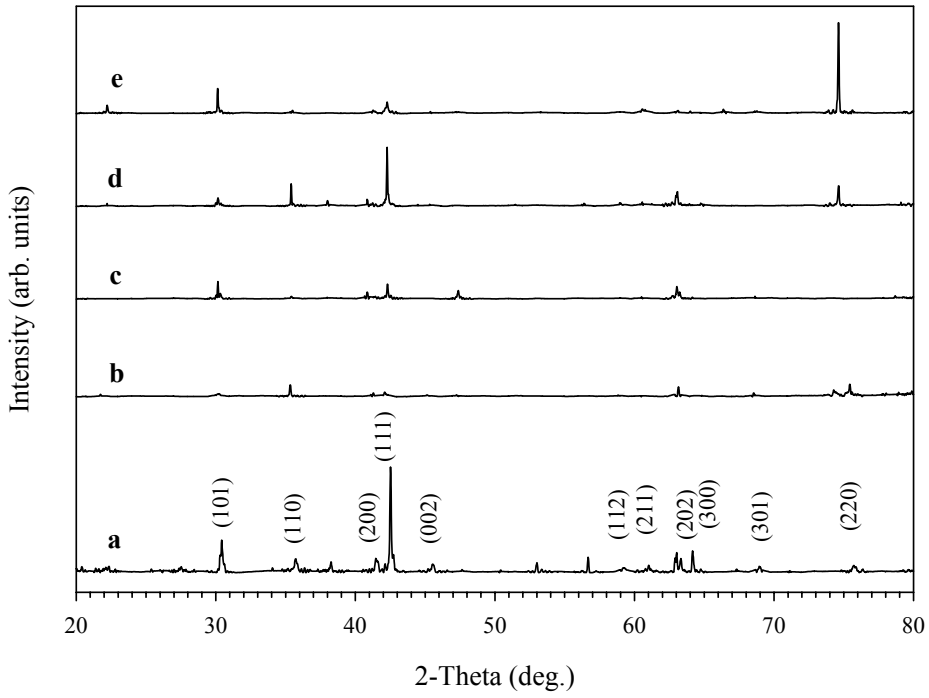

[a] $LaNi_5$ (reference)

[b, c, d, e] non-milled sample

Figure 37. XRD spectra of $LaNi_5$.

$LaNi_5$ was ground with mortar and pestle in the glove box. The three consecutive scans in the XRD (Figure 38) resulted in spectra that involved peaks that matched with the reported peak positions of $LaNi_5$. However, the relative intensity of the observed peaks did not match with the reported ratios, and, inconsistencies within the spectra were observed.

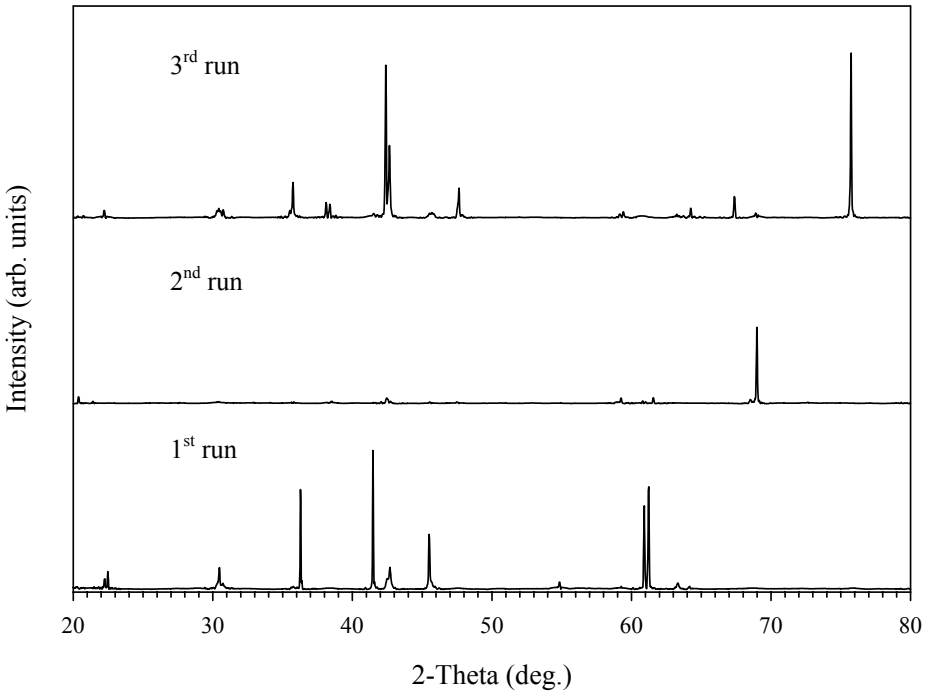

Figure 38. XRD spectra of $LaNi_5$ ground with mortar and pestle.

Five more $LaNi_5$ samples were prepared by ball milling in the Spex8000M for 3, 6, 10, 15 and 30 minutes respectively. The XRD spectra of the samples are given in Figure 39. As the reference, the XRD spectrum of non-milled $LaNi_5$ that most closely matches the expected spectrum is included. The relative intensities of the peaks were observed to approach the reported ratios for $LaNi_5$ as milling duration was increased. This suggests that the normal phase of $LaNi_5$, a $CaCu_5$ phase was formed as the milling proceeded. In contrast, the peaks were observed to lose intensity and broaden, which suggested the formation of an amorphous phase, but, the broadening effect could be because of particle size reduction.

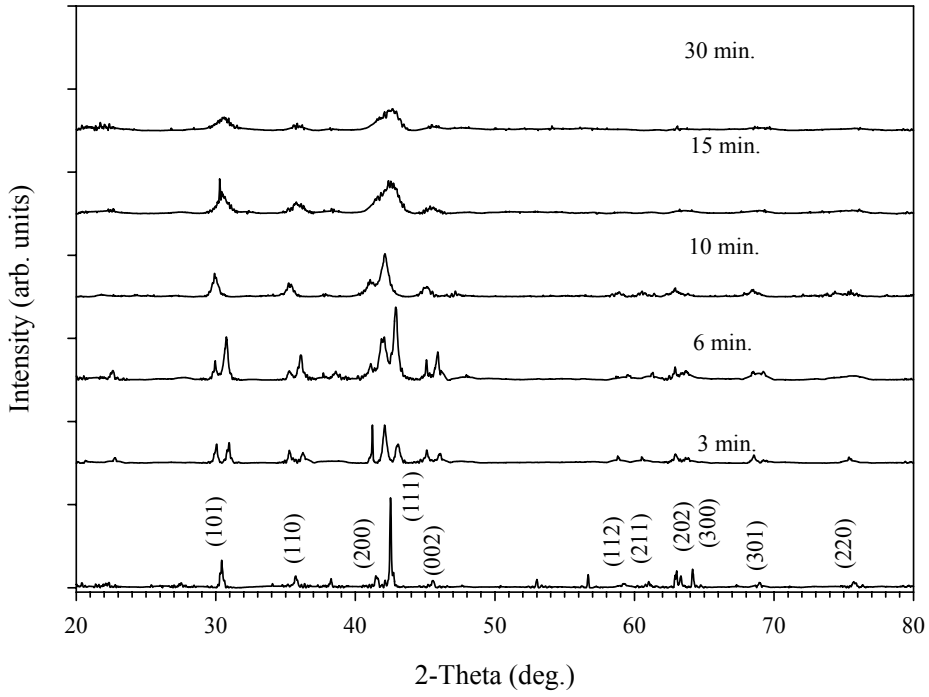

Figure 39. XRD spectra of $LaNi_5$ milled for varying durations.

3.5.2. $LaNi_5$+Al

The XRD spectrum of Al is shown in Figure 40. Samples of $LaNi_5$ mixed with 5.26, 14.29 and 33.33 mole % Al were examined by XRD analysis. The spectrum of $LaNi_5$ with 33 mole % Al is given in Figure 41. In the spectra, aluminum peaks were identified. The Bragg peak for $LaNi_5$ at 42.5º was identified; however, the intensities of other $LaNi_5$ reflection lines were not strong enough to be identified.

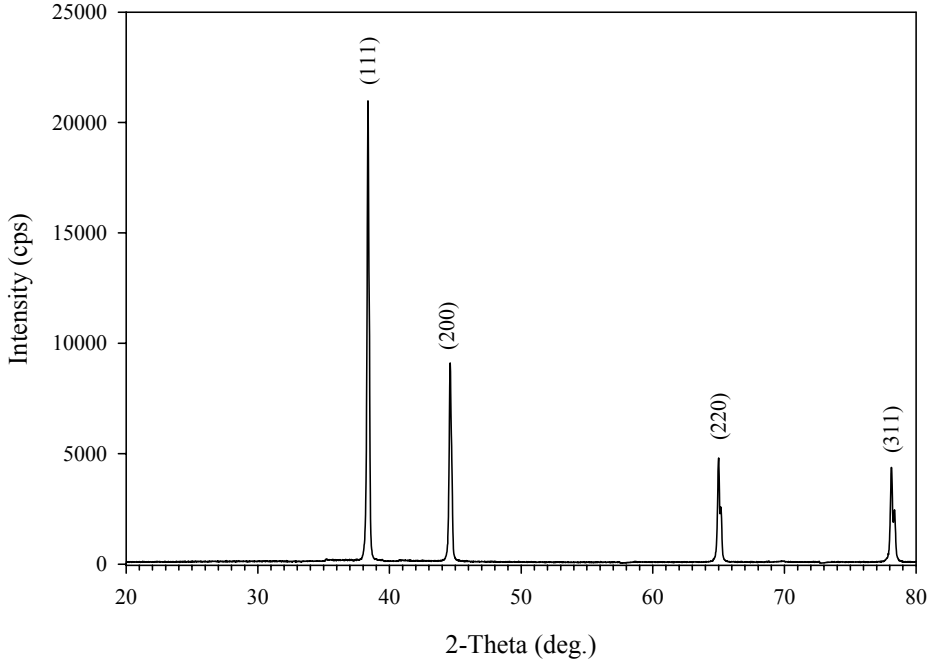

Figure 40. XRD spectrum of aluminum.

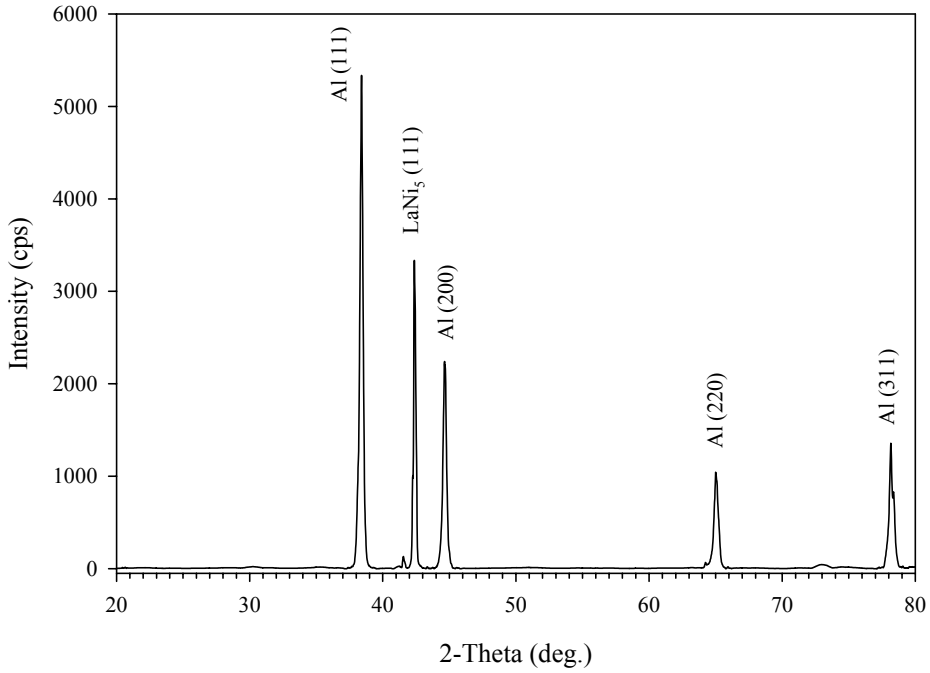

Figure 41. XRD spectrum of non-milled $LaNi_5$ with 33 mole % Al.

After milling the percentages of Al were determined to be 4.74, 12.00 and 47.31 mole %. The XRD spectra of the milled samples are plotted, Figure 42. The intensity of the Al Bragg peak at 38.5º increased with the increased Al content; however, its intensity was less than the Bragg peak of $LaNi_5$. The angle of the Bragg peaks also changed from 42.5º to 42.0º. This suggests the formation of $LaNi_4Al$ for which the angle of the Bragg peak is at 42.0º.

This formation would lead to free Ni through

$$LaNi_5 + Al \rightarrow LaNi_4Al + Ni$$

The Bragg peak for Ni was expected to be at 45.5º, coinciding with one of the lines of $LaNi_5$; therefore, the formation Ni could not be verified. However, for $LaNi_4Al$, a reflection line expected at 44.5º became observable for $LaNi_5$ milled with Al, which also suggests the formation of $LaNi_4Al$ by ball milling. The peak at 44.5º is indicated with a red arrow in the figure.

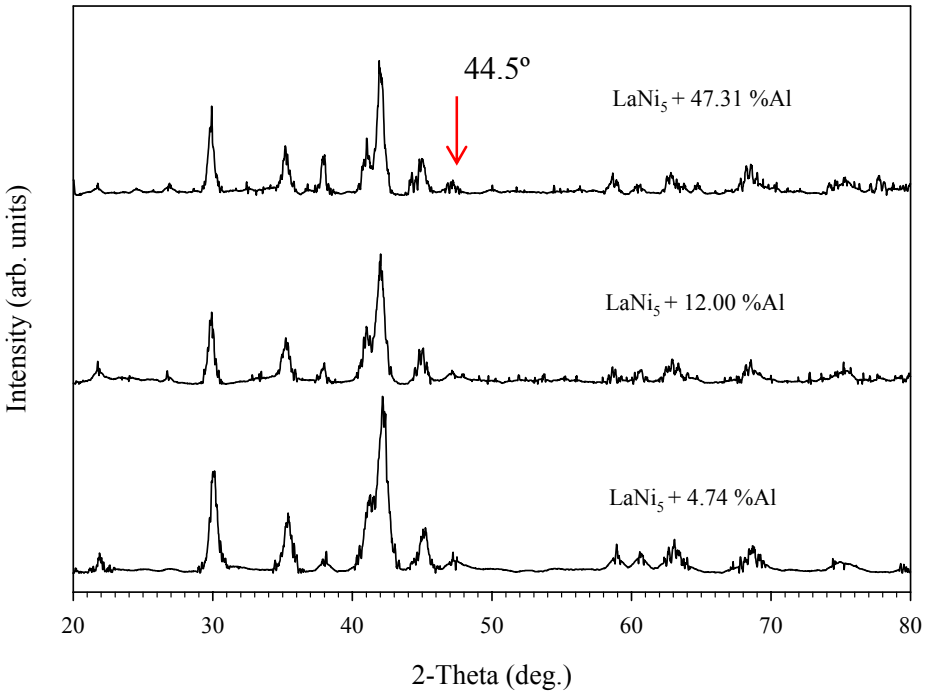

Figure 42. XRD spectra of milled $LaNi_5$ containing Al.

4. CONCLUSIONS

This study has been a contribution to the unexplored field of separation of hydrogen and helium mixtures. The study has concentrated on $LaNi_5$ as the separating agent. In the small scale DSC, it exhibited fast kinetics with H_2 at ambient temperatures and at about 5 atm of pressure. The presence of He negatively influenced these parameters in the small scale. The effect was reduced to a large extent by applying a thin platinum coating on $LaNi_5$; however, this approach would be costly due to the use of Pt in the large scale.

The scaled up analyses of $LaNi_5$ and its derivatives were done with batch and continuous systems. The $LaNi_5$ in the batch system reacted rapidly with H_2 even in the presence of He, provided that the partial pressure of H_2 was high enough.

The continuous U-tube reactor system was successful in producing pure He. However the full capacity of the $LaNi_5$ was not achieved therefore the efficiency was low. The low capacity was due to short residence time of the gaseous reactant in the reactor, with the used equipment. With the addition of flow control equipment, the residence time in the reactor can be increased and the continuous system can be a stronger candidate to be used at the Kennedy Space Center for the recovery of hydrogen and helium.

The XRD analysis of $LaNi_5$ and $LaNi_5Al_x$ suggested that, by ball milling, $LaNi_4Al$ could be produced. However, the extent of conversion was not quantified in this thesis. $LaNi_4Al$, if it had formed, was shown by DSC analysis that, absorbed less H_2 than $LaNi_5$.

LIST OF REFERENCES

1. Rosso, M. J. and Golben, P. M., Journal of the Less Common Metals, 1987. **131**(1-2): p. 283-292.

2. Hampton, M. D. and Slattery, D. K., *Metal Hydrides for Hydrogen Separation, Recovery and Purification, Annual Report for NASA Hydrogen Research at Florida Universities*. 2005, University of Central Florida, Florida Solar Energy Center.

3. Kesting, R. E. and Fritzsche, A. K., *1993*. Polymeric Gas Separation Membranes, New York: John Wiley and Sons.

4. Schweitzer, P. A., *Handbook of Separation Techniques for Chemical Engineers 3rd ed.* 1996, New York: Mc Graw Hill.

5. Liu, B.S. and Au, C. T., Catalysis Letters, 2001. **77**(1-3): p. 67-74.

6. Jordal, K., Bredesen, R., Kvamsdal, H.M., and Bolland, O., Energy, 2004. **29**: p. 1269-1278.

7. Oyama, S. T., Lee, D., Sugiyama, S., Fukuki, K., and Iwasawa, Y., Journal of Materials Science, 2001. **36**: p. 5213-5217.

8. Chiou, J. S. and Paul, D.R., Ind. Eng. Chem. Res., 1988. **27**: p. 2161-2164.

9. Shanin, Y. I., Proc. NATO Advanced Research Workshop on Hydrogen Materials Science and Chemistry of Metal Hydrides, 2001: p. 313-320.

10. Maeland, A.J., in *Hydrides for Energy Storage*, Andersen, A.F., Editor. 1978, Pergamon Press: U.K. p. 19-31.

11. Akiba, E., Current Opinion in Solid State and Materials Science, 1999. **4**: p. 267-272.

12. Fukai, Y., *The Metal-Hydrogen System, Basic Bulk Properties*. 1993, Heidelberg: Springer-Verlag.

13. Fromm, E., *Kinetics of Metal-gas Interactions at Low Temperatures*. 1998, Heidelberg: Springer Verlag.

14. Mintz, M. H. and Bloch, J., Progress in Solid State Chemistry, 1985. **16**: p. 163-194.

15. Bloch, J., Brill, M., Ben-Eliahu, By., and Gavra, Z., Journal of Alloys and Compounds, 1998. **267**: p. 158-166.

16. Van-Vucht, J.H.N., Kuijpers, F.A., and Bruning, H.C.A.M., Philips Research Reports, 1970. **25**: p. 133-140.

17. Mohammed, I.S. and Dakka, A., International Journal of Hydrogen Energy, 2000. **25**: p. 773-777.

18. Sandrock, G., S. Suda, and Schlapbach, L., *Applications*, in *Hydrogen in Intermetallic Compounds II*, Schlapbach, L., Editor. 1992, Springer-Verlag: Heidelberg. p. 197-258.

19. Mitsuishi, N., Sato, S., and Fukada, S., Fusion Engineering and Design, 1995. **28**: p. 362-366.

20. Yukawa, H., Yamashita, D., Ito, S., Morinaga, M., and Yamaguchi, S., Journal of Alloys and Compounds, 2003. **356-357**: p. 45-49.

21. Percheron-Guegan, A. and Welter, J-M., *Preparation of Intermetallics and Hydrides*, in *Hydrogen in Intermetallic Compounds I*, Schlapbach, L., Editor. 1992, Springer-Verlag: Heidelberg.

22. Libowitz, G.G., in *Hydrides for Energy Storage*, A.F. Andersen, A.J.M., Editor. 1978, Pergamon Press: U.K.

23. Reilly, J.J. and Jr., R.H. Wiswall, Inorganic Chemistry, 1968. **7**(11): p. 2254-2256.

24. Hampton, M.D., Juturu, R., and Lomness, J.K., International Journal of Hydrogen Energy, 1999. **24**: p. 981-988.

25. Hampton, M.D. and Lomness, J.K., International Journal of Hydrogen Energy, 1999. **24**: p. 175-187.

26. Tsushio, Y. and Akiba, E., Journal of Alloys and Compounds, 1998. **267**: p. 246-251.

27. Tanaka, S., Clewley, J.D., and Flanagan, T.B., Journal of the Less Common Metals, 1997. **56**: p. 137-139.

28. Boser, O., Journal of the Less Common Metals, 1976. **46**: p. 91-99.

29. Nomura, K. and Akiba, E., Journal of Alloys and Compounds, 1995. **231**: p. 513-517.

30. Lomness, J.K., Hampton, M.D., and Giannuzzi, L.A., International Journal of Hydrogen Energy, 2002. **27**: p. 915-920.

31. Devillers, M., Sirch, M., and Penzhorn, R.-D., Journal of Nuclear Materials, 1993. **207**: p. 53-61.

32. Simonovic, B.R., Mentus, S, Dimitrijevic, R., and Susic, M.V., International Journal of Hydrogen Energy, 1999. **24**: p. 449-454.

33. Libowitz, G.G., Hayes, H.F., and Gibb, T.R.P., Journal of Physical Chemistry, 1958. **62**: p. 76-79.

34. Brundle, C.R., Physical Review Letters, 1978. **40**: p. 972-975.

35. Giza, K., Iwasieczko, W., Drulis, H., Pavlyuk, V.V., and Bala, H., Materials Science and Engineering, 2001. **A303**: p. 158-162.

36. Chen, J., Dou, S.X., and Liu, H.K., Journal of Power Sources, 1996. **63**: p. 267-270.

37. Bowman, R.C., Luo, C.H., Ahn, C.C., Witham, C.K., and Fultz, B., Journal of Alloys and Compounds, 1995. **217**: p. 185-192.

38. Witham, C., Jr, R.C. Bowman, and Fultz, B., Journal of Alloys and Compounds, 1997. **254**: p. 574-578.

39. Rozdzynska-Kielbik, B., Iwasieczko, W., Drulis, H., Pavlyuk, V.V., and Bala, H., Journal of Alloys and Compounds, 2000. **298**: p. 237-243.

40. Mendelsohn, M. H., Gruen, D. M., and Dwight, A.E., Nature, 1977. **269**: p. 45-47.

41. Nishimura, K., Sato, K., Nakamura, Y., Inazumi, C., Oguro, K., Uehara, I., Fujitani, S., and Yonezu, I., Journal of Alloys and Compounds, 1998. **268**: p. 207-210.

42. Luo, S., Luo, W., Clewley, J.D., Flanagan, T.B., and Wade, L.A., Journal of Alloys and Compounds, 1995. **231**: p. 467-472.

43. Flanagan, T.B. and Oates, W.A., *Thermodynamics of Intermetallic Compound-Hydrogen Systems*, in *Hydrogen in Intermetallic Compounds I*, Schlapbach, L., Editor. 1988, Springer-Verlag: Heidelberg.

44. Cohen, R.L. and West, K.W., Journal of Less Common Metals, 1983. **95**: p. 17-23.

45. Uchida, H., International Journal of Hydrogen Energy, 1999. **24**: p. 861-869.

46. Goodell, P.D., Journal of Less Common Metals, 1984. **99**: p. 1-14.

47. Suryanarayana, C., Progress in Materials Science, 2001. **46**: p. 1-184.

48. Msika, E., Latroche, M., Cuevas, F., and Percheron-Guegan, A., Materials Science and Engineering B, 2004. **108**(1-2): p. 91-95.

49. Aoyagi, H., Aoki, K., and Masumoto, T., Journal of Alloys and Compounds, 1995. **231**: p. 804-809.

50. Petrucci, R.H., Harwood, W.S., and Herring, G., *General Chemistry: Principles and Modern Applications, 8th ed.* 2001: Prentice-Hall.

51. http://cst-www.nrl.navy.mil/lattice/spcgrp/hexagonal.html.

52. Peisl, H., *Lattice Strains Due to Hydrogen in Metals*, in *Hydrogen in Metals I*, G. Alefeld, J.V., Editor. 1978, Springer-Verlag: Heidelberg. p. 53-74.

53. Seta, S. and Uchida, H., Journal of Alloys and Compounds, 1995. **231**: p. 448-453.

54. Yvon, K. and Fischer, P., *Crystal and Magnetic Structures of Ternary Metal Hydrides: A Comprehensive Review*, in *Hydrogen in Intermetallic Compounds I*, Schlapbach, L., Editor. 1992, Springer-Verlag: Heidelberg. p. 87-138.

55. Andersen, A.F., in *Hydrides for Energy Storage*, A.F. Andersen, A.J.M., Editor. 1978, Pergamon: U.K. p. 61-72.

56. Furrer, A., Fischer, P., Halg, W., and Schlapbach, L., in *Hydrides for Energy Storage*, A.F. Andersen, A.J.M., Editor. 1978, Pergamon Press: U.K. p. 73-82.

57. Smith, W.F., *Foundations of Materials Science and Engineering*. 2004, New York: Mc Graw Hill.

58. Hashimoto, Y., Asano, K., and Iijima, Y., Materials Transactions, 2002. **43**(11): p. 2696-2702.

59. Jurczyk, M., Smardz, K., Rajewski, W., and Smardz, L., Materials Science and Engineering, 2001. **A303**: p. 70-76.

60. Smardz, L., Smardz, K., Jurczyk, M., and Jakubowicz, J., Materials Science and Engineering, 2000. **313**: p. 192-200.

61. M. J. Rosso, P. M. Golben, Journal of the Less Common Metals, 1987. **131**(1-2): p. 283-292.

62. Corre, S., Bououdina, M., Kuriyama, N., Fruchart, D., and Adachi, G., Journal of Alloys and Compounds, 1999. **292**: p. 166-173.

63. H. Fujii, S. Munehiro, K. Fujii, S. Orimo, Journal of Alloys and Compounds, 2002. **330-332**: p. 747-751.

64. Flanagan, T.B., in *Proceedings of the International Symposium on Hydrides for Energy Storage*, Maeland, A.F.A.a.A.J., Editor. 1978, Pergamon: Oxford.